Received: 9 March 2023 | Revised: 24 April 2023 | Accepted: 26 April 2023

DOI: 10.1111/jnc.15843

Journal of Neurochemistry JNC The Official Journal of the International Society for Neurochemistry WILEY

ORIGINAL ARTICLE

Peripheral and central neuroplasticity in a mouse model of endometriosis

Joel Castro[1,2] | Jessica Maddern[1,2] | Andelain Erickson[1,2] | Andrea M. Harrington[1,2] | Stuart M. Brierley[1,2,3]

[1]Visceral Pain Research Group, College of Medicine and Public Health, Flinders Health and Medical Research Institute (FHMRI), Flinders University, Bedford Park, South Australia, Australia

[2]Hopwood Centre for Neurobiology, Lifelong Health Theme, South Australian Health and Medical Research Institute (SAHMRI), Adelaide, South Australia, Australia

[3]Discipline of Medicine, University of Adelaide, Adelaide, South Australia, Australia

Correspondence
Joel Castro, Visceral Pain Research Group, Level 7, South Australian Health and Medical Research Institute (SAHMRI), North Terrace, SA 5000, Australia.
Email: joel.castro@sahmri.com

Funding information
Australian Research Council, Grant/Award Number: ARC Discovery Project (DP220101269), Discovery Early Career Research Award (DE130100223 and Discovery Project (DP180101395); Hospital Research Foundation, Grant/Award Number: PhD Scholarship (SAPhD000242018); National Health and Medical Research Council, Grant/Award Number: Development Grant (APP2014250), Ideas Grant # APP1181448 and Investigator Leadership Grant (APP2008727)

Abstract

Chronic pelvic pain (CPP) is the most debilitating symptom of gynaecological disorders such as endometriosis. However, it remains unclear how sensory neurons from pelvic organs affected by endometriosis, such as the female reproductive tract, detect and transmit nociceptive events and how these signals are processed within the central nervous system (CNS). Using a previously characterized mouse model of endometriosis, we investigated whether the increased pain sensitivity occurring in endometriosis could be attributed to (i) changes in mechanosensory properties of sensory afferents innervating the reproductive tract, (ii) alterations in sensory input from reproductive organs to the spinal cord or (iii) neuroinflammation and sensitization of spinal neural circuits. Mechanosensitivity of vagina-innervating primary afferents was examined using an ex vivo single-unit extracellular recording preparation. Nociceptive signalling from the vagina to the spinal cord was quantified by phosphorylated MAP kinase ERK1/2 immunoreactivity. Immunohistochemistry was used to determine glial and neuronal circuit alterations within the spinal cord. We found that sensory afferents innervating the rostral, but not caudal portions of the mouse vagina, developed mechanical hypersensitivity in endometriosis. Nociceptive signalling from the vagina to the spinal cord was significantly enhanced in mice with endometriosis. Moreover, mice with endometriosis developed microgliosis, astrogliosis and enhanced substance P neurokinin-1 receptor immunoreactivity within the spinal cord, suggesting the development of neuroinflammation and sensitization of spinal circuitry in endometriosis. These results demonstrate endometriosis-induced neuroplasticity occurring at both peripheral and central sites of sensory afferent pathways. These findings may help to explain the altered sensitivity to pain in endometriosis and provide a novel platform for targeted pain relief treatments for this debilitating disorder.

Abbreviations: ANOVA, analysis of variance; CNS, central nervous system; CPP, chronic pelvic pain; CTB, cholera toxin subunit B; DAB, diaminobenzidine; DDH, deep dorsal horn; DGC, dorsal grey commissure; DH, dorsal horn; DRG, dorsal root ganglia; Endo, endometriosis; ERK1/2, extracellular signal-regulated kinase 1/2; GFAP, glial fibrillary acidic protein; HRP, horseradish peroxidase; I.P., intraperitoneal; Iba1, ionized calcium-binding adaptor protein; IBS, irritable bowel syndrome; IC/BPS, interstitial cystitis/bladder pain syndrome; IR, immunoreactive; IVC, individually ventilated cages; LS, lumbosacral; LSN, lateral spinal nucleus; MAP kinase, mitogen-activated protein kinase; MRI, magnetic resonance imaging; NK1r, neurokinin 1 receptor; OAB, overactive bladder syndrome; pERK, phosphorylated MAP kinase ERK 1/2; ROI, region of interest; SDH, superficial dorsal horn; SEM, standard error of the mean; SPN, sacral parasympathetic nucleus; T-PBS, triton-TX phosphate-buffered saline; VFH, von Frey hair.

Joel Castro and Jessica Maddern contributed equally to this work.

KEYWORDS
central neuroinflammation and sensitization, chronic pelvic pain, endometriosis, hypersensitivity, peripheral and central neuroplasticity, vagina-innervating afferents

1 | INTRODUCTION

Endometriosis is a chronic inflammatory gynaecological disorder affecting approximately 10% of females of reproductive age (Koninckx et al., 2019; Zito et al., 2014), which imparts an economic load of almost $80 billion/year in the USA alone (Soliman et al., 2016). Chronic pelvic pain (CPP) is the most debilitating symptom experienced by women with endometriosis, however, adequate treatments are lacking. Current research into the mechanisms underlying pain in endometriosis primarily focuses on endometriotic lesions and their inflammatory environment as the source of CPP (Maddern et al., 2020; Morotti et al., 2014). However, surgical removal of endometriotic lesions does not reliably provide pain relief (Abbott et al., 2004; Sutton et al., 1994). Additionally, endometriosis patients are commonly co-diagnosed with gynaecological comorbidities, including uterine fibroids, adenomyosis and polycystic ovarian syndrome (Chen et al., 2021; Decter et al., 2021), together with other visceral comorbidities such as irritable bowel syndrome (IBS) and overactive bladder syndrome (OAB) (Surrey et al., 2018); suggesting complex lesion-independent mechanisms that evoke chronic changes in pain signalling or processing are involved.

Sensory neurons that project from peripheral tissues to the central nervous system (CNS) are the first step in the pain pathway. How sensory neurons detect and transmit pain from pelvic organs affected by endometriosis remains unclear. This presents a limiting factor when developing treatments for endometriosis-associated CPP. The female reproductive tract is innervated by sensory afferents arising in the nodose, pelvic, hypogastric and pudendal nerves (Monica Brauer & Smith, 2015). Both the pelvic and hypogastric sensory afferents innervating the female reproductive tract of healthy rats are known to be activated by mechanical and chemical stimuli (Berkley et al., 1990; Berkley, Hubscher, & Wall, 1993; Berkley, Robbins, & Sato, 1993; Robbins et al., 1990). More recently, we further characterized the mechanosensory profile of pelvic sensory afferents innervating the vagina of healthy mice, demonstrating their ability to detect a range of mechanical stimuli (Castro et al., 2021). Moreover, we found that activation of these pelvic sensory afferents leads to activation of neurons within the dorsal horn of the spinal cord, as well as pain-related behaviours in vivo (Castro et al., 2021). We also demonstrate that the visceromotor responses to vaginal distension were enhanced in two mouse models of endometriosis, indicating the induction of a chronic pain state (Castro et al., 2021; Maddern et al., 2021). Despite these advances, how endometriosis modulates the detection, transmission and processing of sensory signalling from the vagina remains to be determined.

A major factor in the development of many chronic visceral pain disorders, including IBS and OAB, is the altered plasticity of sensory afferents innervating visceral organs, leading to the development of sensory afferent hypersensitivity to mechanical stimuli. Mechanical hypersensitivity results in an increase in nociceptive signalling from the periphery to the CNS. Furthermore, chronic peripheral afferent hypersensitivity is known to induce neuroplastic changes within the CNS circuitry, resulting in persistent CPP (Berkley, 2005; Brierley & Linden, 2014; Grundy et al., 2019; Scholz & Woolf, 2007). Similar neuroplastic changes have been suggested to occur in endometriosis (Arnold et al., 2012; Berkley et al., 2005; Maddern et al., 2020), where long-term exposure to proinflammatory cytokines within the peritoneal cavity is hypothesized to activate and sensitize sensory afferents innervating pelvic organs and endometriotic lesions (Asante & Taylor, 2011; Laux-Biehlmann et al., 2015). However, whether the sensory afferents innervating the vagina develop mechanical hypersensitivity in endometriosis, and how this may contribute to enhanced transmission of nociceptive signals to the CNS to induce a chronic pain state, remains to be determined.

In this study, we investigated whether (i) primary afferents innervating the female reproductive tract of the mouse develop mechanical hypersensitivity in endometriosis; (ii) the sensory input from these organs to the spinal cord is augmented in endometriosis; and (iii) if neuroinflammation and sensitization of neural circuits develop in the regions of the spinal cord receiving altered nociceptive input from reproductive organs. This article describes key alterations within both the peripheral and central nervous system which may help explain the altered sensitivity to pain associated with endometriosis.

2 | MATERIALS AND METHODS

2.1 | Animals

The Animal Ethics Committees of the South Australian Health and Medical Research Institute (SAHMRI) and Flinders University approved all experiments involving animals (ethics number SAM342). All experiments conformed to the relevant regulatory standards and the ARRIVE guidelines. Virgin female C57BL/6J mice at 6–8 weeks of age acquired from an in-house C57BL/6J breeding programme (JAX strain #000664; originally purchased from The Jackson Laboratory (breeding barn MP14)) within SAHMRI's specific and opportunistic pathogen-free animal care facility were used for all experiments. Mice were group-housed (maximum five mice per cage) within individual ventilated cages (IVC), which were filled with coarse-chip dust-free aspen bedding (PURA®; Cat# – ASPJMAEB-CA). These cages were stored on IVC racks in specific housing rooms within a temperature-controlled environment of 22°C and a 12 h light/12 h

dark cycle. Mice had free access to LabDiet® JL Rat and Mouse/Auto6F chow (Cat# 5K52) and autoclaved reverse osmosis purified water.

2.2 | Study design

A total of 54 female mice were used for data presented in this study, with 28 mice allocated to the 'Sham' group and 26 mice allocated to the 'Endo' group. No animals were excluded in this study. The animals used in this study were arbitrarily assigned prior to surgical induction of either Sham or Endo on Day 0 (d0). Blinding was achieved throughout the experiments, and data analysis was carried out by each experimenter after being blinded to the treatment group via the use of mouse ID numbers only. The total number of mice used in each individual data set is specified within individual figure legends (identified as N). An estimated sample size of $N = 6$ was determined based on previously published studies of similar nature that used a power value of 0.80 and an alpha error probability of 0.05, with a moderate confidence interval of 0.41708 and standard error of 0.21280 (Castro et al., 2021; Castro et al., 2022; Jiang et al., 2021).

2.3 | Study timeline

Endometriosis (or Sham) was surgically induced in ovariectomized mice at 6 weeks of age and allowed to develop for a minimum of 8 weeks before mice were killed, and tissue collected for the experimental protocols used in this study. All tissue used in this study was collected between 8 and 10 weeks of endometriosis development. A schematic representation demonstrating the timeline for surgical interventions and the timing of tissue collection for experimental methods is shown in Figure 1.

2.4 | Mouse model of endometriosis and sham control mice

We used our previously established autologous mouse model of surgically induced endometriosis (Castro et al., 2021). Briefly, female mice were ovariectomized to deplete endogenous steroid production and administered with an intraperitoneal (i.p.) injection of 100 μg/kg estradiol benzoate (or Progynon-B) to maintain steady levels of circulating oestrogen and minimize any difference related to the stage of the oestrous cycle (Burns et al., 2012; Castro et al., 2021; Somigliana et al., 1999). Seven days after ovariectomy and oestradiol benzoate injection, mice were surgically induced with endometriosis. For this, the mouse's uterine horns were exposed, excised and transferred into a dissecting dish containing ice-cold sterile phosphate-buffered saline supplemented with penicillin (100 U/mL) and streptomycin (100 μg/mL, Sigma-Aldrich). Uterine horns were longitudinally opened, with 5 × 2 mm fragments of uterine horn tissue removed using a 2 mm biopsy punch (Kai Medical, KAI00010). Three fragments were sutured back into the same mouse on alternate mesenteric cascade arteries that supply the small intestine, and the remaining two pieces were sutured on either side of the

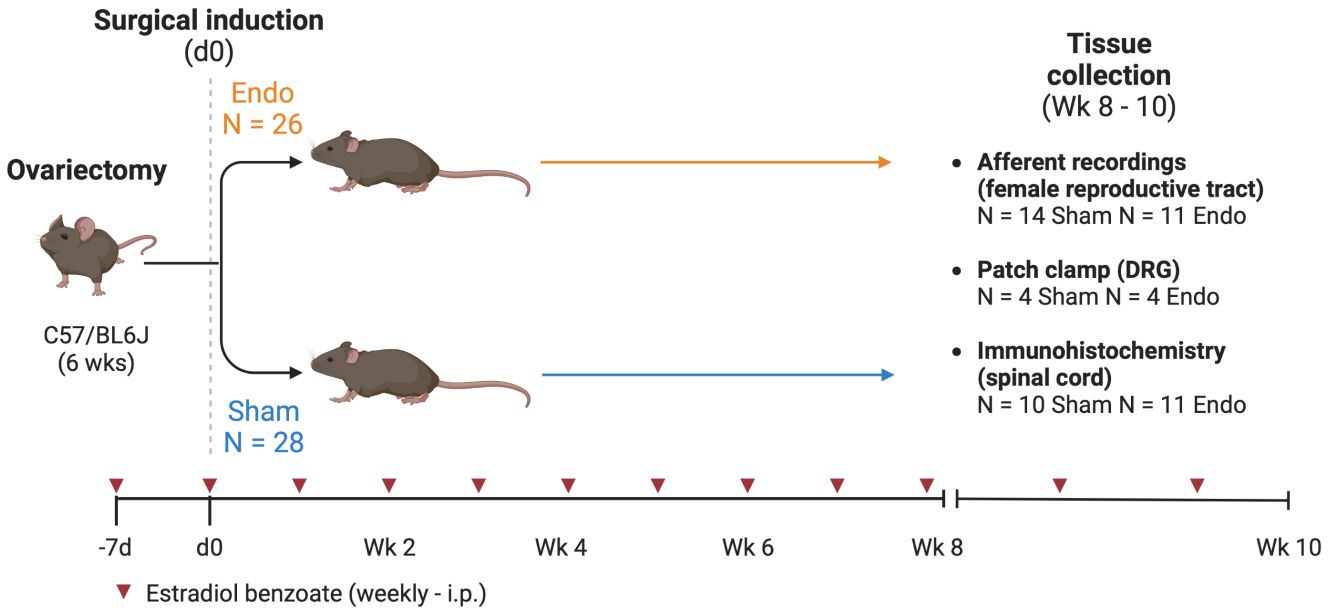

FIGURE 1 Schematic representation of the timeline of surgical interventions and model development for tissue collection performed in this study. Female C57BL/6J mice were ovariectomized at 6 weeks of age, 1 week (−7 days) prior to either Sham ($N = 28$) or Endo ($N = 26$) induction surgery at day 0 (d0). All mice were injected weekly with estradiol benzoate (i.p. red arrows) to maintain steady levels of circulating oestrogen. All tissue was collected between 8 and 10 weeks of model development for experiments including afferent recordings ($N = 14$ Sham and $N = 11$ Endo mice), patch clamp recordings ($N = 4$ Sham and $N = 4$ Endo mice) and immunohistochemistry ($N = 10$ Sham and $N = 11$ Endo mice). The number of mice used for each experiment can be found within individual data sets, represented by N.

uterus (Castro et al., 2021). To maintain steady levels of circulating oestrogen and minimize any difference related to the stage of the oestrous cycle, all mice were given an i.p. injection of 100 μg/kg oestradiol benzoate (or Progynon-B) immediately after surgery, and once a week for up to 10 weeks (Castro et al., 2021). To generate Sham mice, which were used as controls in this study, the same procedure was followed, but fat was sutured instead of uterine horn tissue, within the small intestine mesentery cascade and alongside the uterus.

We have previously characterized this mouse model of endometriosis and showed that mice with fully established endometriosis (8–10 weeks after surgery) developed endometriotic lesions, neuroangiogenesis and an enhanced inflammatory environment within the peritoneal cavity (Castro et al., 2021). Moreover, we demonstrated that mice with endometriosis also displayed: (i) enhanced sensitivity to pain evoked by vaginal and colorectal distension, (ii) altered bladder function and (iii) increased sensitivity to cutaneous thermal and mechanical stimuli, with no effect on spontaneous behaviour (Castro et al., 2021).

2.5 | Ex vivo afferent recording preparation from pelvic and pudendal nerves innervating the female reproductive tract

On the day of experimentation, Sham and Endo mice (8–10 weeks after surgery, mice with fully developed endometriosis) were humanely killed by CO_2 inhalation and the whole female reproductive tract was removed. Afferent recordings from pelvic and pudendal nerves innervating the vaginal area were performed as previously described (Castro et al., 2020). Briefly, intact female reproductive organs (vagina and uterus) were removed along with the attached neurovascular bundle containing pelvic and pudendal nerves. The whole tissue was transferred to ice-cold Krebs solution (in mM: 117.9 NaCl, 4.7 KCl, 25 $NaHCO_3$, 1.3 NaH_2PO_4, 1.2 $MgSO_4(H_2O)7$, 2.5 $CaCl_2$ and 11.1 D-glucose); and following further dissection, the distal and central portions of the female reproductive organs were opened longitudinally. The tissue was pinned flat, mucosal side up, in a specialized organ bath. The neurovascular bundle containing the pelvic or the pudendal nerve was extended from the tissue compartment into a recording compartment where they were laid onto a mirror. The pelvic or pudendal nerve was dissected away from the neurovascular bundle and from the nerve sheath surrounding the nerve under a dissecting microscope. Using fine forceps, the nerve trunk was teased apart into 6–10 bundles, which were individually placed onto a platinum recording electrode. A separate platinum reference electrode rested on the mirror in a small pool of Krebs solution adjacent to the recording electrode. Action potentials, generated by mechanical stimuli applied to the afferent's receptive field, were recorded, as previously described (Castro et al., 2020) by a differential amplifier, filtered and sampled (20 kHz) using a 1401 interface (Cambridge Electronic Design).

2.5.1 | Mechanosensory profile of pelvic and pudendal afferents innervating the vagina

Receptive fields were identified by systematically stroking the mucosal surface of the vagina with a stiff brush to activate all subtypes of mechanoreceptors. As previously described (Castro et al., 2020), in order to study the baseline mechanosensory properties of afferents innervating a particular receptive field of the female reproductive tract, three distinct mechanical stimuli were tested, these stimuli included: (i) static probing with calibrated von Frey hairs (vfh; 2 g force; applied three times for a period of 3 s); (ii) mucosal stroking of the vaginal surface with calibrated vfh (10–1000 mg force; applied 10 times each); or (iii) circular stretch (5 g; applied for a period of 1 min). Stretch was applied using a claw made from bent dissection pins attached to the tissue adjacent the afferent receptive field and connected to a cantilever system with thread (Castro et al., 2020). Weights were applied to the opposite side of the cantilever system to initiate stretch. Only circular, and not longitudinal, stretch was tested in this study, as previously described (Castro et al., 2020).

2.5.2 | Statistical analysis of afferent recording data

Action potentials were analysed offline using the Spike 2 (version 5.21) software (Cambridge Electronic Design) and discriminated as single units based on distinguishable waveforms, amplitudes and durations. Data are expressed as mean ± standard error of the mean (SEM). n = the number of afferents recorded, N = the number of animals used for those specific experiments. Data were statistically compared using GraphPad Software Prism 9 software and, where appropriate, were analysed using an unpaired Student's t-test with two tails for two groups of equal variances or using the Mann–Whitney nonparametric test for two groups with unequal variances, or one- or two-way analysis of variance (ANOVA) with Bonferroni post hoc tests. Additionally, differences in the proportion of pudendal afferents responding to any given stimuli between Sham and Endo mice were analysed using Chi-square test. T and p values are indicated within the results or figure legends where appropriate. Differences were considered statistically significant at $^{*}p < 0.05$, $^{**}p < 0.01$, $^{***}p < 0.001$ and $^{****}p < 0.0001$.

2.6 | Patch clamping studies on dorsal root ganglia (DRG) neurons innervating the vagina

2.6.1 | Identification of vagina-innervating DRG neurons by retrograde labelling

Retrograde labelling was performed to identify dorsal root ganglia (DRG) neurons innervating the vagina as previously described (Castro et al., 2020). Briefly, nerve tracer (cholera toxin subunit B (CTB) conjugated to AlexaFluor® 488) was injected at five different sites into the vaginal wall of anesthetized Sham and Endo mice, as

previously described (Castro et al., 2020). Four days after vaginal tracing, mice were humanely killed via CO_2 inhalation, and lumbosacral (LS; L5-S1) DRG were removed. Harvested DRG were digested with a mix of 3.3 mg/mL Collagenase II (GIBCO, Thermo Fisher Scientific, #17101015) and 4.7 mg/mL Dispase II (GIBCO, Thermo Fisher Scientific, #17105041) at 37°C for 30 min, then 3.3 mg/mL Collagenase II for 10 min, as previously described (Bellono et al., 2017; Brierley et al., 2011; Castro et al., 2013, 2017, 2019; Castro et al., 2020; Inserra et al., 2017; Osteen et al., 2016). After enzymatic digestion, DRG were mechanically dissociated via trituration through fire-polished Pasteur pipettes. Neurons were then resuspended and spot plated onto 15 mm coverslips coated with laminin (20 μg/mL; Sigma-Aldrich, #L2020) and poly-D-lysine (800 μg/mL; Thermo Fisher Scientific). Finally, coverslips were incubated at 37°C in 5% CO_2 for 2–3 h to allow neurons to adhere before flooding with 1.7 mL complete DMEM as previously described (Bellono et al., 2017; Brierley et al., 2011; Castro et al., 2013, 2017, 2019; Castro et al., 2020; Inserra et al., 2017; Osteen et al., 2016).

2.6.2 | Whole-cell current-clamp electrophysiology of vagina-innervating DRG neurons

Dissociated DRG neurons isolated from vagina-traced mice were recorded in current-clamp mode on day 1 post-culturing, as previously described (Castro et al., 2020). Briefly, neurons were held at −70 mV for 15 ms, hyperpolarized by a −20 pA current injection for 475 ms, then held at −70 mV for 100 ms. Stepwise depolarizing pulses in increments of 10, 25 or 50 pA (475 ms) were applied from holding potential of −70 mV with 2 s repetition intervals to determine the rheobase (minimum amount of current required to fire an action potential) and number of action potentials at two times rheobase, as previously described (Castro et al., 2020). Intracellular solution contained (in mM): 135 KCl; 2 $MgCl_2$; 2 MgATP; 5 EGTA-Na; 10 HEPES-Na; adjusted to pH 7.3. Extracellular (bath) solution contained (in mM): 140 NaCl; 4 KCl; 2 $MgCl_2$; 2 $CaCl_2$; 10 HEPES; 5 D-glucose; adjusted to pH 7.4. Standard wall borosilicate glass pipettes (OD × ID × length: 1.5 mm × 0.86 mm × 7.5 cm, Harvard, cat # 64-0792) were pulled and fire polished to 5–10 MΩ using a P-97 (Sutter Instruments) pipette puller. Exclusion criteria: For current-clamp recordings, neurons were not recorded if the resting membrane potential was more depolarized than −40 mV as this is an indicator of poor cell health, as previously described (Castro et al., 2020). Recordings were amplified with Axopatch 200A, digitized with Digidata 1322A, sampled at 20 kHz, filtered at 5 kHz, recorded with pCLAMP 9 software (Molecular Devices) and analysed in Clampfit 10.3.2 (Molecular Devices), GraphPad Software Prism 9 software and IBM SPSS Statistics v25, as previously described (Castro et al., 2020). T and *p* values are indicated within the results or figure legends where appropriate. Neurons patched in this study were small to medium in size, with an average diameter of 27.4 ± 0.45 μm. Liquid junction potential was not corrected.

2.7 | Identification of spinal cord dorsal horn neurons activation evoked by vagina distension in vivo

To identify the spatial relationship between the spinal projections of DRG sensory neurons innervating the vagina, and the dorsal horn (DH) spinal neurons activated by vaginal distension, we combined retrograde labelling of the vagina using CTB conjugated to AlexaFluor® 488 (CTB-AF488), with immunofluorescence labelling of the neuronal activation marker phosphorylated MAP kinase ERK 1/2 (pERK) as per below.

2.7.1 | Retrograde tracing to identify spinal projections of DRG sensory neurons innervating the vagina

A small aseptic abdominal incision was made in anesthetized (isoflurane 2–4% in oxygen) Sham or Endo mice. 0.5% CTB-AF488 nerve tracer, diluted in 0.1 M phosphate buffer (Thermo Fisher Scientific), was injected into the vaginal wall using a Hamilton syringe attached to a 23-gauge needle. Injections sites covered the cervix region and the fundus (~2 mm immediately caudal to the cervix). In addition, the lower portion of the vagina was traced by injecting the dye into the vaginal muscle through the vaginal opening (~2 mm immediately rostral the vaginal opening). Tracer was injected at five different sites within those regions (3 μL/injection site). Following tracer injection, the abdominal incision was sutured closed, and analgesic (Buprenorphine; 2.7 μg/30 g) and antibiotic (Ampicillin; 50 mg/kg) treatment was given subcutaneously as mice regained consciousness. Mice were housed individually and monitored for recovery over 7 days.

2.7.2 | Activation and identification of spinal cord neurons activated by vagina distension

Seven days after retrograde labelling, mice were subjected to noxious vaginal distension in vivo to activate dorsal horn neurons within the spinal cord, as previously described (Castro et al., 2020). Briefly, a balloon catheter was inserted into either the vaginal canal (~3 mm length) of anesthetized Sham or Endo mice. Mice were removed from the isoflurane chamber, and on regaining consciousness, the balloon was distended to 60 mm Hg (5 × 30 s distension with 10 s deflation) via a syringe attached to a sphygmomanometer pressure gauge. After the final distension, mice were given an anaesthetic overdose and by 5 min, had undergone transcardial perfuse fixation with 4% paraformaldehyde in 0.1 M phosphate buffer, as previously described (Castro et al., 2020). After complete perfusion, lumbosacral (L6-S2) spinal cord segments were removed and post-fixed in 4% paraformaldehyde in 0.1 M phosphate buffer at 4°C for 18–20 h. At this point, samples were re-assigned a sample number to ensure downstream processing, and analysis was performed in a blinded fashion. Spinal cord segments

were cryoprotected, frozen in 100% optimal cutting temperature (OCT) compund, and subsequentially cryosectioned in a serial fashion (10 μm thick) and placed over five gelatin-coated slides for immunofluorescence labelling (InstrumeC Uberfrost Printer Slides). In addition to pERK labelling for quantification, a serial slide from each mouse was processed using immunofluorescence to identify vaginal CTB AF488 retrograde tracing and pERK labelling to visualize the spatial relationship between the vaginal-innervating neurons and dorsal horn neurons activated from noxious distension.

2.7.3 | pERK immunostaining and imaging

After being sectioned, slides were air dried for 1 h and washed with 0.2% Triton-TX 100 (Sigma Aldrich) in 0.1 M phosphate-buffered saline (T-PBS) to remove excess OCT. Slides were blocked with 5% normal chicken serum (CHBX00100, Applied Biological Products) diluted in T-PBS to inhibit non-specific binding of secondary antibodies. Sections were then incubated overnight at room temperature, in primary antibody Phospho-p44.42 MAPK ERK1/2 (pERK) (1:100) (4370, Cell Signalling). Sections were washed in T-PBS followed by incubation with secondary rabbit IgG conjugated to AF594 (1:200) (A21442; Thermo Fischer) for 1 h at room temperature. Following a final wash in T-PBS, sections were mounted using Prolong Gold Antifade and cover slipped for imaging.

Fluorescence was visualized using a confocal laser scanning microscope (Leica TCS SP8X, Wetzlar, Germany). Representative images of retrograde labelling (AF488) location and pERK immunostaining (AF594) were obtained at 1024 × 1024 pixels using 20× magnification lens, and between stacks sequential, line average five scanning with the following excitation and emission settings: AF488 excitation line 495 (9.78% white light laser power) emission 505–541 hybrid detector (198.6% gain) and AF594 excitation line 483 (64.1% white light laser power) emission 596–953 hybrid detector (727% gain).

2.8 | Quantification of spinal cord dorsal horn neurons activation evoked by vagina distension in vivo

Phosphorylated MAP kinase ERK 1/2 (pERK) was detected using primary antibody (pERK; 1:800, MAB4370, Cell Signalling Technology) in Antibody Diluent (S0809, Agilent DAKO) with 3,3′-diaminobenzidine (DAB), followed by horseradish peroxidase (HRP) secondary antibody staining. Non-specific binding of secondary antibodies was blocked with Serum-Free Protein Block (X0909, Agilent DAKO). Tissue sections were pre-incubated with primary antisera for 1 h, washed and incubated in Envision FLEX Peroxidase-blocking Reagent (GV823, Agilent DAKO), followed by Envision FLEX HRP Polymer (GV823, Agilent DAKO) for HRP binding. Negative controls were prepared as per above but omitting primary antibody. Sections were then washed in wash buffer (GC807, DAKO Omnis, Agilent) before a 10-min incubation in EnVision FLEX Substrate Working Solution (DAB) for staining, as previously described (Castro et al., 2020). DAB/HRP-stained slides were imaged using a 3DHistech Panoramic 250 Flash II slide scanner at 40×, as previously described (Castro et al., 2020). Images of individual sections from L6–S2 regions were taken using digital pathology viewing software (QuPath 0.1.2) and analysed using ImageJ software, as previously described (Castro et al., 2020). The images were not manipulated in any way.

Neuronal counts were analysed from previously saved digital photomicrographs, with only neurons with intact nuclei counted, as previously described (Castro et al., 2020). The number of pERK-immunoreactive (IR) dorsal horn neurons/animal was obtained from a minimum of nine sections/animal/spinal segment (L6-S2). The total number of pERK-IR neurons from the dorsal horn overall and selectively from dorsal horn regions was then analysed across all mice. The selective dorsal horn regions analysed were defined as the superficial dorsal horn (SDH, Lamina LI-II), deep dorsal horn (DDH, lamina LIII-V), dorsal grey commissure (DGC), lateral spinal nucleus (LSN) and the sacral parasympathetic nucleus (SPN, only in S1-S2 spinal segments). Selection of the dorsal horn regions was based on previous published work (Castro et al., 2020; Lein et al., 2007) and the Allen Spinal Cord Atlas (available from https://mousespinal.brain-map.org). Data were analysed using an unpaired Student's *t*-test with two tails for two groups of equal variances or using the Mann–Whitney non-parametric test for two groups with unequal variances to compare the number of pERK-IR neurons between Sham and Endo mice in different regions of the dorsal horn. T and *p* values are indicated within the results or figure legends where appropriate. Differences were considered statistically significant at $^{*}p < 0.05$, $^{**}p < 0.01$, $^{***}p < 0.001$ and $^{****}p < 0.0001$. Data are expressed as mean ± SEM. Figures were prepared in GraphPad Prism 9 software. N represents number of animals per group, while n represents the number of neurons or independent observations.

2.9 | Quantification of microglia and astrocyte activation within the spinal cord

The degree of glia cell activation within the spinal cord was examined by visualizing spinal microglia cells activation (via Ionized calcium-binding adaptor protein (Iba1) immunofluorescence) and astrocyte activation (via glial fibrillary acidic protein (GFAP) immunofluorescence) as previously reported (Adaes et al., 2017; Echeverry et al., 2008) and detailed below.

2.9.1 | Immunohistochemical labelling for GFAP and Iba1

Spinal cord tissue collected, and serially sectioned, from mice following vaginal distension was analysed for GFAP and Iba1 labelling. Slides were post-fixed in 10% formalin for 1 min and briefly

rinsed in deionized distilled water. Slides underwent automated immunohistochemical labelling via the DAKO Omnis (Agilent Technologies Australia). First, slides were incubated in Envision FLEX TRS Low pH target retrieval solution (citrate buffer, pH 6.1; K8005, Agilent DAKO) at 97°C for 30 min followed by wash buffer (GC807, DAKO Omnis, Agilent). Protein block was then achieved using a Serum-free Protein Block (X0909, Agilent DAKO). Either rabbit anti-GFAP: 1:15000 (Low pH) Polyclonal Rabbit Anti-Glial Fibrillary Acidic Protein (Code Z0334 DAKO) or Rabbit IbA-1 1: 2500 (Low pH) Polyclonal Rabbit Anti-IbA-1 Protein (Code 019-19741 WAKO) was then applied as the primary antibody for 1 h, followed by wash buffer. Slides were then blocked for 3 min in Envision FLEX Peroxidase-blocking Reagent (GV823, Agilent DAKO) and washed. HRP binding was achieved by 20 min of incubation with Envision FLEX HRP polymer (GV823, Agilent DAKO). Following a wash, Envision FLEX Substrate working solution (DAB) was applied for 10 min. Finally, slides were washed and incubated for 3 min with Haematoxylin ready-to-use solution (K8018, Agilent DAKO). Slides were then dehydrated in alcohol and cleared in xylene before being mounted with dibutyl phthalate polystyrene xylene (DPX, Sigma-Aldrich) and cover slipped.

2.9.2 | Imaging and analysis

Sections were imaged using a Hamamatsu Photonics NanoZoomer 2.0-HT Digital Slide Scanner using x40 magnification and bright-field settings. All images were imported into QuPath (QuPath image analysis software version 2.2) and standardized to image type (bright-field H-DAB) with colour deconvolution stains set standard across all images. Regions of interest (ROI) measurements were made from the entire dorsal horn (unilateral) and within selected dorsal horn regions: superficial dorsal horn (SDH) laminae (LI-II; with the ventral edge of LII identified by the gradient change between the translucent band of LII and dense band of LIII), deep dorsal horn (DDH; inclusive of LIII-LV) and the dorsal grey commissure (DGC). These areas were selected owing to previous observations showing that the afferent input converging on the DDH, SDH and DGC could be modulated by targeting nociceptors expressed within the vagina tissue (Castro et al., 2020). The 'detect positive staining' analysis module in the QuPath software was used to measure the percentage total ROI stained with 'positive pixels' above threshold using standardized settings (down-sample factor 2, Gaussian sigma 1, haematoxylin threshold 'negative' 0.1 OD units and DAB threshold 'positive' 0.3–0.6 OD units). Thresholds were calibrated empirically to accommodate slight variations in stain intensity. Measurements of positive pixel area (μm^2), as well as the perimeter of each area measured (μm), were collected from 7 to 10 sections per mouse. After all images were analysed in this fashion, they were re-identified and sorted into their experimental groups (Sham or Endo mice). The total area (μm^2) covered by pixels above threshold per ROIs per experimental sample was plotted and analysed using GraphPad Prism 9 software.

The total number of GFAP- and Iba1-positive cells with intact cell bodies were manually counted within all regions analysed. To determine if morphological changes could relate to the area covered by each Iba1-positive cell within each region of the spinal cord ('*area of staining covered per region*'), further analysis was performed by manually outlining each intact cell (including an intact cell body and visible cell processes) visible within all regions analysed ('*area covered by each cell*'). The 'detect positive staining' analysis module in the QuPath software was used to measure the total area stained with 'positive pixels' above threshold using standardized settings (down-sample factor 2, Gaussian sigma 0.1, haematoxylin threshold 'negative' 0.1 OD units and DAB threshold 'positive' 0.5 OD units). To determine whether morphological changes could specifically relate to the area covered by the processes of each Iba1-positive cell ('*area covered by cell's processes*'), the area of the cell soma (measured using the 'positive cell detection' analysis module in the QuPath software with standardized nucleus parameters: sigma 1 μm, minimum area 10 μm^2 and nucleus DAB OD mean 'positive' 0.5 units) was deducted from the total area of the cell.

Data were graphed and analysed within GraphPad Prism 9 software using unpaired Student's *t*-test with two tails for two groups of equal variances, or the Mann–Whitney test for two groups of unequal variances, to compare between Sham and Endo mice in different regions of the dorsal horn. T and *p* values are indicated within the results or figure legends where appropriate. Differences were considered statistically significant at $^{*}p<0.05$, $^{**}p<0.01$, $^{***}p<0.001$ and $^{****}p<0.0001$. Data are expressed as mean ± SEM. N represents number of animals per group, while n represents the number of neurons or independent observations.

2.10 | Histological assessment of neuronal circuits within the spinal cord

Changes occurring within specific dorsal horn nociceptive circuits associated with the development of endometriosis were examined by visualizing the degree of neurokinin 1 receptor (NK1r) immunolabelling within the spinal cord dorsal horn as it has been suggested that there is a significant up-regulation of the NK1r on neurons in the dorsal spinal cord following long-term visceral inflammation (Palecek et al., 2003).

2.10.1 | Spinal cord neurokinin 1 receptor (NK1r) immunofluorescence

Spinal cord from Sham and Endo mice were collected, frozen in 100% OCT, subsequentially cryosectioned in a serial fashion (10 μm thick) and placed over five gelatin-coated slides for immunofluorescence labelling (InstrumeC Uberfrost Printer Slides). After being sectioned, slides were air dried for 1 h and washed with 0.2% Triton-TX 100 (Sigma Aldrich) in 0.1 M phosphate-buffered saline (T-PBS) to remove excess OCT. Non-specific

binding of secondary antibodies was blocked with 5% normal chicken serum (CHBX0010; Applied Biological Products) diluted in T-PBS. Tissue sections were incubated with rabbit anti-NK1r antisera (1:2000; S8305 Sigma-Aldrich, Merck; RRID: AB_261562) for 18 h at room temperature, diluted in T-PBS. Sections were then washed in T-PBS and incubated for 1 h at room temperature with chicken anti-rabbit conjugated to AlexaFluor594 (1:200, A-21442 Thermo Fisher Scientific; RRID: AB_2535860). Sections were then washed in T-PBS before mounting in Prolong Gold Antifade and cover slipped. Slides were allowed to dry for 24 h prior to visualization. The anti-NK1r was raised against the synthetic peptide corresponding to the C-terminal of NK1r of rat origin (amino acids 393–407). This sequence is highly conserved in mouse, guinea pig and human NK1r, but diverges in other tachykinin receptor subtypes NK2r and NK3r. Immunoblotting shows that this antibody recognizes a 46 kb band (manufacturers' technical information), and staining for NK1r using this antibody has previously been reported (Polgár et al., 2010).

2.10.2 | Imaging and analysis

Fluorescence was visualized using an epifluorescent microscope (Olympus BX51) using a 10X objective with standardized exposure of 2 s. Images were processed using FIJI (NIH) and Corel Draw 2017 (CorelDraw Graphic Suite 2017, Corel) software. Other than making standardized adjustments for contrast and brightness, the images were not manipulated in any way.

Using Image-J FIJI (NIH) analysis module, all images were scaled to 1.54 pixels/μm and the NK1r-AF594 immunoreactivity was manually selected by thresholding images to 36/255–38/25. The total area (μm^2) covered by pixels above threshold was then measured using the Image-J measurement module. Measurements were made from the entire dorsal horn (unilateral) and within selected dorsal horn regions: superficial dorsal horn (SDH) laminae (LI-II; with the ventral edge of LII identified by the gradient change between the translucent band of LII and dense band of LIII), deep dorsal horn (DDH; inclusive of LIII-LV) and the dorsal grey commissure (DGC). These measurements were made from five sections of spinal cord per spinal segment per mouse and averaged across mice from each experimental group.

Data were graphed and analysed within GraphPad Prism 9 software using unpaired Student's *t*-test with two tails for two groups of equal variances to compare between Sham and Endo mice in different regions of the dorsal horn. T and *p* values are indicated within the results or figure legends where appropriate. Differences were considered statistically significant at $^{*}p<0.05$, $^{**}p<0.01$, $^{***}p<0.001$ and $^{****}p<0.0001$. Data are expressed as mean ± SEM. *N* represents number of animals per group, while *n* represents the number of sections per animal.

3 | RESULTS

3.1 | Mechanosensory properties of primary sensory afferents innervating the vagina via the pelvic nerve are altered in endometriosis

It is widely accepted that mechanical hypersensitivity of sensory primary afferents innervating visceral organs is a key characteristic linked to chronic pain disorders, such as irritable bowel syndrome and interstitial cystitis (Castro et al., 2013; Castro et al., 2017; Dang et al., 2008; DeBerry et al., 2014; Grundy et al., 2019; Grundy, Harrington, et al., 2018; Harrington et al., 2012). Using our recently developed ex vivo single-unit recording preparation (Castro et al., 2020), we investigate whether sensory afferents innervating pelvic organs, such as the female reproductive tract, develop mechanical hypersensitivity during endometriosis.

We characterized the mechanosensory profile of pelvic afferents innervating the vaginal area of Sham mice and mice with endometriosis (Endo mice). Pelvic afferent nerve terminals had small (~0.5 mm) punctate receptive fields throughout the length of the

FIGURE 2 Pelvic afferents innervating the vagina of mice with endometriosis are hypersensitive to mechanical stimuli. (a) Schematic diagram of the female reproductive tract showing distribution of pelvic nerve afferent receptive fields along the vagina of (i) Sham mice and (ii) mice with endometriosis (Endo mice). (b–d) Grouped data from ex vivo single-unit extracellular nerve recording preparations showing the mechanosensory properties of pelvic afferents from Sham mice (blue symbols) and Endo mice (orange symbols), in response to three different mechanical stimuli. Compared to Sham mice, Endo mice displayed significantly increased responses to (b) focal compression with 2 g von Frey hair (vfh) filament, with significant differences observed at the following compression stimuli: 400 mg ($^{*}p=0.0192$), 600 mg ($^{*}p=0.0273$), 1400 mg ($^{**}p=0.0014$) and 2000 mg ($^{*}p=0.0281$) with no difference at 7 mg ($p\geq0.9999$), 160 mg ($p=0.5288$) and 1000 mg ($p=0.1291$) (two-way ANOVA with Bonferroni post hoc comparison test, with $^{*}p<0.05$ and $^{**}p<0.01$ indicated on the graph); (c) fine stroking of the vaginal mucosa surface with 10–1000 mg calibrated vfh filaments, with a significant difference observed at 1000 mg stoking pressure ($^{***}p=0.0003$) and no difference at 10 mg ($p=0.6162$), 200 mg ($p=0.4810$) and 500 mg ($p=0.0550$, Sidak's multiple-comparisons tests, with $^{***}p<0.001$ indicated on the graph); and (d) circular stretch of the whole tissue ($^{*}p=0.0387$, unpaired Student's *t*-test). All receptive fields studied from the pelvic nerve were responsive to all three stimuli. (e) Grouped data showing the response of pelvic vaginal afferents to circular stretch of the vagina in Sham mice (blue symbols) and Endo mice (orange symbols). (i) Afferent firing induced by circular stretch lasted significantly longer in Endo mice compared to Sham mice ($^{*}p=0.0162$, Mann–Whitney test). (ii) The time taken for circular stretch to induce action potential firing (latency of the response) is reduced in Endo mice compared to Sham mice ($^{*}p=0.0379$, Mann–Whitney test). (iii) The number of action potentials generated by circular stretch is partially, but not significantly, increased in Endo mice compared to Sham mice ($p=0.2299$, Mann–Whitney test). Grouped data are from $n=11$ afferents from $N=7$ Sham mice and from $n=9$ afferents from $N=5$ Endo mice. Data represent mean ± SEM. NS = Not Significant.

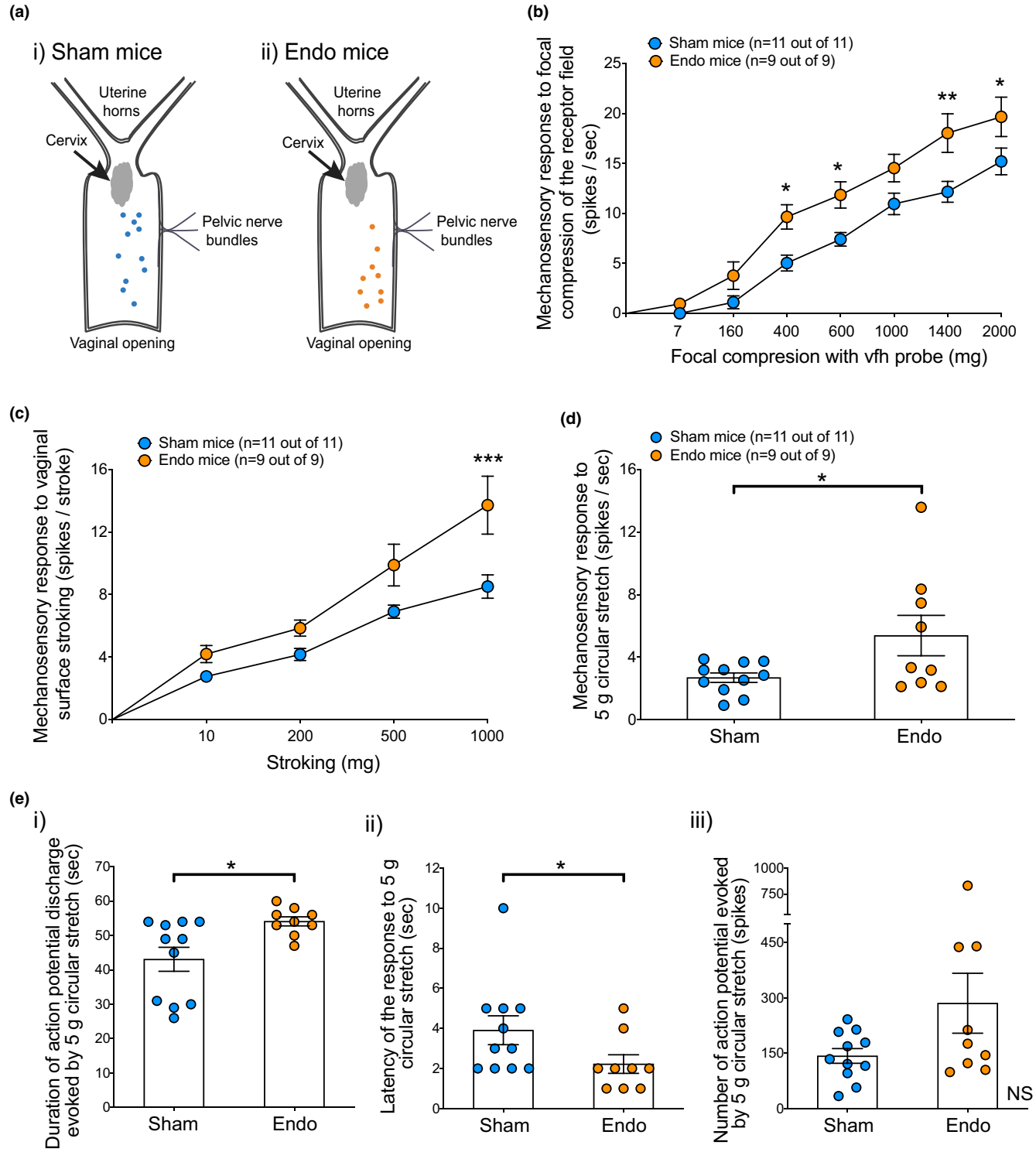

vagina, from which action potentials were evoked in response to a variety of mechanical stimuli as previously described (Castro et al., 2020). Receptive fields of pelvic afferents from Sham and Endo mice displayed similar distributions throughout the vagina (Figure 2ai,ii).

We examined the response of pelvic afferents to three different mechanical stimuli as previously described (Castro et al., 2020) and found that pelvic afferents innervating the vagina of mice with endometriosis were hypersensitive to all three mechanical stimuli compared to afferents from Sham mice (Figure 2b–d). Specifically, vaginal afferent hypersensitivity was manifested by a significant increase in the action potential generation in response to: (i) focal compression with a calibrated 2 g von Frey hair (vfh) filament (Figure 2b; Bonferroni's multiple-comparison tests, $p = 0.0014$–>0.9999, for full details, see Figure 2b), (ii) fine stroking of the vaginal lumen surface with calibrated 10–1000 mg vfh (Figure 2c; Sidak's multiple-comparison tests, $p = 0.0003$–0.6162, for full details, see Figure 2c) and (iii) circular stretch of the whole tissue, applied via

a cantilever system compared to Sham mice (Figure 2d; $t=2.230$, df = 18, $p=0.0387$, Sham: 2.687 ± 0.3003 vs. Endo: 5.385 ± 1.293, unpaired *t*-test). Additional characterization of the response to circular stretch showed that pelvic afferents from Endo mice fired action potentials for a significatively longer period than that observed during circular stretch of the vagina of Sham mice (Figure 2ei; $U=18.50$, $p=0.0162$, Sham: 43.09 ± 3.486 vs. Endo: 54.11 ± 1.328, Mann–Whitney test). This was accompanied by an earlier response (Figure 2eii; $U=23$, $p=0.0379$, Sham: 3.909 ± 0.7193 vs. Endo: 2.222 ± 0.4648, Mann–Whitney test), and a trend to fire more action potentials throughout the duration of the stimuli (Figure 2eiii; $U=33$, $p=0.2299$, Sham: 142.7 ± 19.96 vs. Endo: 285.7 ± 81.36, Mann–Whitney test), than afferents from Sham mice.

3.2 | Mechanosensory properties of primary sensory afferents innervating the vagina via the pudendal nerve are not altered in endometriosis

Using a modified version of the ex vivo afferent recording preparation (Castro et al., 2020), we were able to record the activity of primary afferents innervating the lower portion of the vagina via the pudendal nerve. We found that pudendal afferent nerve terminals had small (~0.5 mm) punctate receptive fields from which action potentials were evoked in response to mechanical stimuli. These receptive fields were found at the caudal end of the vagina and were similarly distributed in both Sham and Endo mice (Figure 3a).

We examined the mechanosensory properties of pudendal nerve fibres from a particular receptive field using the same three distinct mechanical stimuli described above. This included the effect of: (i) static focal compression of the receptive field with a calibrated vfh (Figure 3b), (ii) fine stroking of the vaginal lumen surface with calibrated 10–1000 mg vfhs (Figure 3c) and (iii) 5 g circular stretch of the vagina (Figure 3d). Interestingly, we found that not all afferents responded (firing of action potentials) to all stimuli tested. Most of the afferents responded to focal compression of the receptive field (100% on Sham mice (15 out of 15 afferents) and 91% on Endo mice (10 out of 11 afferents)); around two-thirds of the afferents responded to fine stroking of the vaginal lumen surface (80% on Sham mice (12 out of 15 afferents) and 63.6% on Endo mice (7 out of 11 afferents)), and approximately half of the afferents responded to circular stretch of the vagina (53.3% on Sham mice (9 out of 15 afferents) and 45.5% on Endo mice (5 out of 11 afferents)) (Figure 3b–d). Despite this heterogeneity, Sham and Endo mice have a similar proportion of afferents responding to any of the stimuli tested (Figure 3b, df = 1.417, 1, z = 1.191, $p=0.2337$, Chi-square test; Figure 3c, df = 0.8637, 1, z = 0.9292, $p=0.3527$, Chi-square test; and Figure 3d, df = 0.5403, 1, z = 0.7350, $p=0.4623$, Chi-square test). Moreover, afferents innervating the vagina via the pudendal nerve did not show changes in mechanosensory properties with the development of endometriosis (Figure 3b–d). This was apparent with a similar number of action potentials, between Sham and Endo mice, generated in response to (i) focal compression with von Frey hair (vfh) filament (Figure 3b; Bonferroni's multiple-comparison tests, $p=0.2556$–>0.9999, for full details, see Figure 3b), (ii) fine stroking of the vaginal lumen surface (Figure 3c; Sidak's multiple-comparison tests, $p=0.8092$–0.9997, for full details, see Figure 3c) and (iii) circular stretch of the whole tissue (Figure 3d; $t=0.02656$, $df=12$, $p=0.9792$, Sham: 4.796 ± 0.9626 vs. Endo: 4.837 ± 1.182, unpaired Student's *t*-test). Moreover, the profile of the response to circular stretch of vaginal-innervating pudendal afferents was similar in Sham and Endo mice (Figure 3ei, $U=20$, $p=0.7657$, Sham: 49.89 ± 2.412 vs. Endo: 50.40 ± 3.265, Mann–Whitney test; Figure 3eii, $t=0.3481$, $df=12$, $p=0.7338$, Sham: 3.444 ± 0.4747 vs. Endo: 3.200 ± 0.3742, unpaired Student's *t*-test; Figure 3eiii, $U=21$, $p=0.8716$, Sham: 193.8 ± 32.97 vs. Endo: 235.6 ± 77.71, Mann–Whitney test).

3.3 | Excitability of lumbosacral sensory DRG neurons innervating the mouse vagina is not altered in endometriosis

To investigate whether the mechanical hypersensitivity of pelvic afferents innervating the vagina of mice with endometriosis translates

FIGURE 3 Mechanosensitivity of pudendal afferents innervating the vagina is not altered in mice with endometriosis. (a) Schematic diagram of the female reproductive tract showing the distribution of pudendal nerve afferent receptive fields along the vagina of (i) Sham mice and (ii) mice with endometriosis (Endo mice). (b–d) Grouped data from ex vivo single-unit extracellular nerve recording preparations showing mechanosensory properties of pudendal afferents from Sham mice (blue symbols) and Endo mice (orange symbols) in response to three different mechanical stimuli. *Note*: Not all receptive fields studied responded to all three stimuli. Only responded afferents are included in the data. The number of afferents responding to a particular stimulus is indicated on graph's legend. Sham and Endo mice exhibited similar responses to (b) focal compression with von Frey hair (vfh) filaments (7 mg: $p\geq0.9999$, 160 mg: $p\geq0.9999$, 400 mg: $p=0.2556$, 600 mg: $p=0.6819$, 1000 mg: $p\geq0.9999$, 1400 mg: $p\geq0.9999$ and 2000 mg: $p\geq0.9999$, two-way ANOVA with Bonferroni post hoc comparison test), (c) fine stroking of the vaginal mucosa surface with 10–1000 mg calibrated vfh filaments (10 mg: $p=0.8092$, 200 mg: $p=0.8353$, 500 mg: $p=0.9898$ and 1000 mg: $p=0.9997$, Sidak's multiple-comparisons tests) and (d) circular stretch of the whole tissue ($p=0.9792$, unpaired Student's *t*-test). Moreover, Sham and Endo mice have a similar proportion of afferents responding to any of the stimuli tested (Figure 3b, $p=0.2337$; Figure 3c, $p=0.3527$; and Figure 3d, $p=0.4623$, Chi-square test). (e) Grouped data showing the response of pudendal vaginal afferents to circular stretch of the vagina in Sham mice (blue symbols) and Endo mice (orange symbols). Analysis of the profile of the response to circular stretch showed pudendal afferents innervating the vagina of Endo mice have similar (i) duration ($p=0.7657$, Mann–Whitney test), (ii) latency ($p=0.7338$, unpaired Student's *t*-test) and (iii) magnitude ($p=0.8716$, Mann–Whitney test) to that displayed by Sham mice. Grouped data are from a total $n=15$ pudendal afferents from $N=7$ Sham mice and $n=11$ afferents from $N=6$ Endo mice. Data represent mean ± SEM. NS = Not Significant.

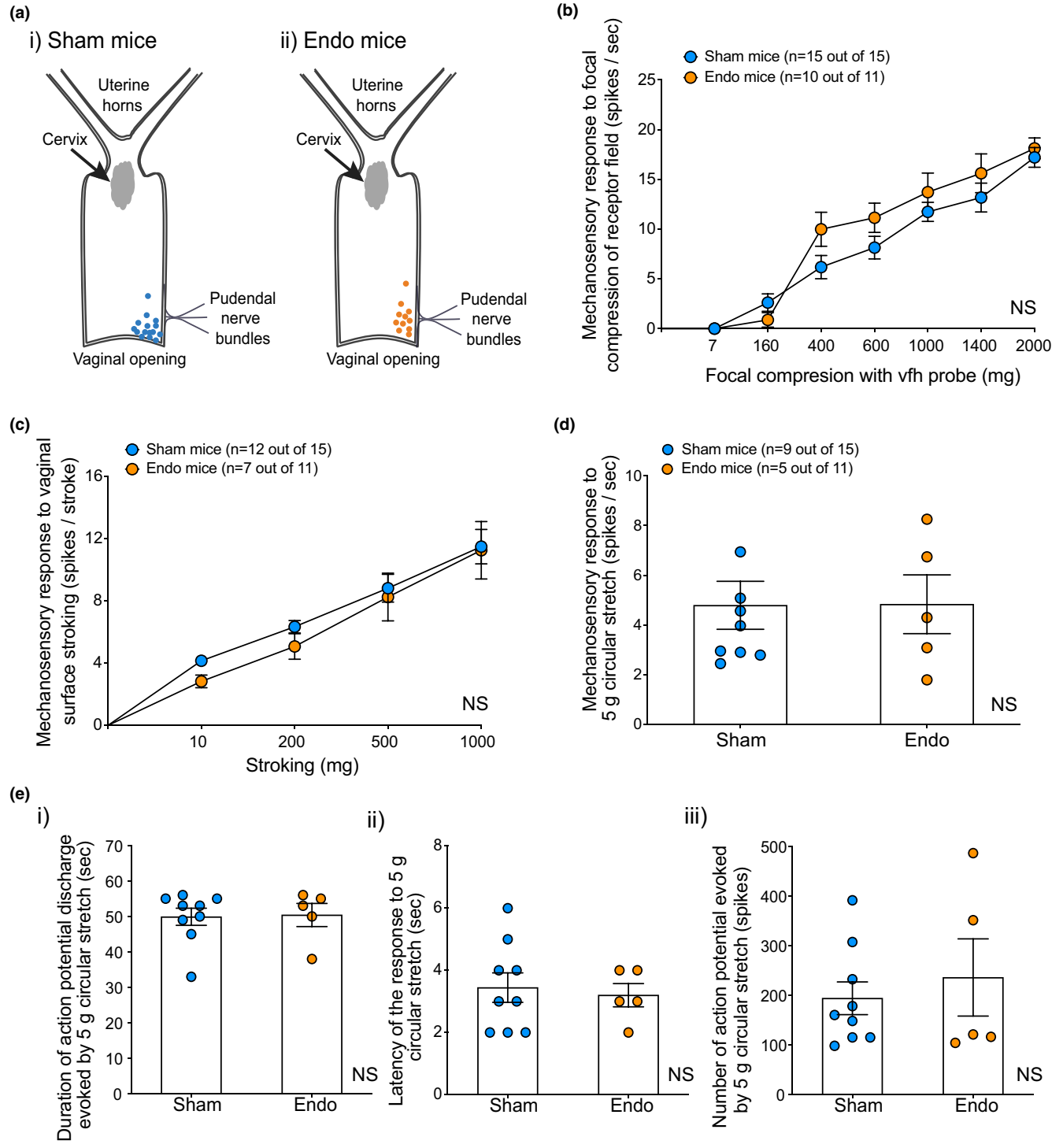

to an increase in the excitability of DRG sensory neurons innervating the vagina, we performed in vitro patch clamp recordings in cultured lumbosacral (LS; L5-S1) DRG sensory neurons innervating the vagina of Sham mice and Endo mice. Vagina-innervating DRG neurons were visually identified in culture by the presence of the fluorescent nerve tracer CTB AlexaFluor®488, which was retrogradely injected in the vagina wall 4 days prior to culture, as previously described (Castro et al., 2020).

Our in vitro current-clamp experiments showed that vagina-innervating sensory neurons cultured from Sham and Endo mice required a similar amount of current to fire an action potential, also known as the rheobase (Figure 4a,b; $U = 1233$, $p = 0.2809$, Sham: 218.4 ± 37.43 vs. Endo: 213.1 ± 34.85, Mann–Whitney test). In addition, we found that vagina-innervating sensory neurons cultured from Sham and Endo mice were similar in size (Figure 4ci; $t = 0.06847$, $df = 104$, $p = 0.9455$, Sham: 27.33 ± 0.5208 vs. Endo: 27.39 ± 0.7328, unpaired Student's t-test) and displayed similar electrophysiological properties, including resting membrane potential (Figure 4cii; $t = 0.9372$, $df = 104$, $p = 0.3508$, Sham: -53.69 ± 0.9355 vs. Endo: -52.56 ± 0.7629, unpaired Student's t-test) and membrane capacitance (Figure 4ciii; $U = 1342$, $p = 0.6952$, Sham: 30.08 ± 1.053

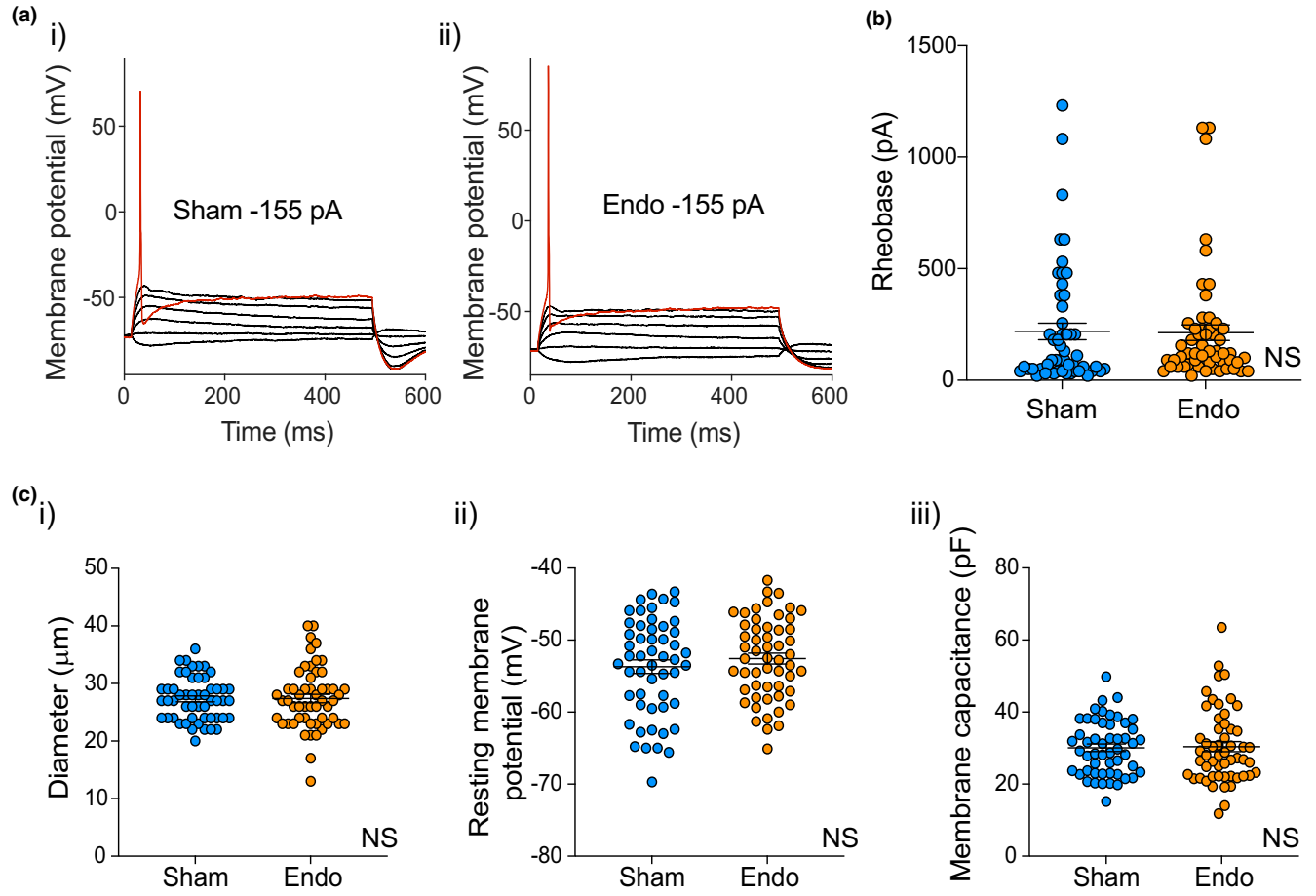

FIGURE 4 Excitability of lumbosacral sensory DRG neurons innervating the mouse vagina is not altered in endometriosis. (a) Original whole-cell current-clamp recordings of a single retrogradely traced vagina-innervating lumbosacral (LS; L5-S1) DRG sensory neuron during current step protocols. Each line represents a 10 pA increase in current. In these examples, the measured threshold current required to elicit an action potential (red trace) in vagina-innervating sensory neuron cultured from (i) Sham mice and (i) Endo mice is 155 pA, indicating no changes in neuronal excitability. (b) Grouped data showing no differences between the average current threshold (rheobase) in vagina-innervating DRG neurons cultured from Sham (blue symbols) and Endo mice (orange symbols) ($p = 0.2809$, Mann–Whitney test on natural log-transformed rheobase). (c) Vagina-innervating sensory DRG neurons cultured from Sham (blue symbols) and Endo mice (orange symbols), displayed similar (i) cell diameters ($p = 0.9455$, unpaired Student's *t*-test); (ii) resting membrane potential ($p = 0.3508$, unpaired Student's *t*-test) and (iii) membrane capacitance ($p = 0.6952$, Mann–Whitney test). Data are from $n = 52$ neurons from $N = 4$ Sham mice, and $n = 54$ neurons from $N = 4$ Endo mice). Data represent mean ± SEM. NS = Not Significant.

vs. Endo: 30.39 ± 1.403, Mann–Whitney test). Overall, these results indicate that vagina-innervating neurons cultured from Sham and Endo mice demonstrated similar excitability, displaying the same ability to fire action potentials when stimulated, in vitro.

3.4 | Mice with endometriosis displayed enhanced nociceptive signalling in the dorsal horn of the spinal cord in response to vaginal distension in vivo

It has been hypothesized that women with endometriosis developed chronic changes in nociceptive signalling within the CNS. This has also been suggested to occur in animal models of endometriosis (Berkley et al., 2005; Brawn et al., 2014; Dodds et al., 2016; Maddern et al., 2020). Given the peripheral mechanical hypersensitivity characterized in Endo mice, we next aimed to determine whether this translated to enhanced nociceptive signalling into the CNS. To do this, we examined the number of phosphorylated-MAP-kinase-ERK immunoreactive (pERK-IR) dorsal horn neurons within the LS (L6-S2) spinal cord, evoked by noxious distension of the vagina, as previously described (Castro et al., 2020).

To confirm the distribution of vagina-innervating sensory nerve terminals within the LS (L6-S2) spinal cord, we examined their location relative to dorsal horn neurons, visualized by pERK immunoreactivity, in response to noxious distension of the vagina (Figure 5). We found that retrogradely labelled vagina-innervating central nerve terminals were primarily distributed within the superficial dorsal horn (SDH; laminae LI-II), the dorsal grey commissure (DGC) and projecting within lateral tracts of Lissauer and within the sacral parasympathetic nucleus (SPN) of the spinal cord dorsal horn (Figure 5, magenta colour). In addition, pERK-IR neurons were primarily

localized within these regions following in vivo noxious distension of the vagina (Figure 5, blue colour). Detailed imaging of these regions showed that pERK-IR dorsal horn neurons were physically surrounded by vaginal afferent central projections (Figure 5a,b).

We then quantified neuronal activation evoked by noxious distension of the vagina within the same regions of the LS (L6-S2) spinal cord (Figure 6) and found that Endo mice displayed a significantly increased number of pERK-IR neurons in response to noxious vaginal distension, compared to Sham mice (Figure 6ci; U = 1106, $p = 0.0022$, Sham: 25.39 ± 1.218 vs. Endo: 34.10 ± 1.979, Mann–Whitney test). Analysis of specific areas within the lumbosacral spinal cord showed that, compared to Sham mice, Endo mice had significantly increased numbers of pERK-IR neurons in the SDH (Figure 6cii; *U = 1162*, $p = 0.0059$, Sham: 5.648 ± 0.3519 vs. Endo: 7.361 ± 0.4266, Mann–Whitney test), followed by the DDH (Figure 6ciii; $t = 2.227$, $df = 113$, $p = 0.0279$, Sham: 7.981 ± 0.4513 vs. Endo: 9.918 ± 0.7138, unpaired Student's *t*-test), DGC (Figure 6civ; *U = 1169*, $p = 0.0105$, Sham: 7.981 ± 0.5511 vs. Endo: 11.20 ± 0.8425, Mann–Whitney test) and LSN (Figure 6cv; *U = 1268*, $p = 0.0315$, Sham: 2.481 ± 0.2941 vs. Endo: 3.787 ± 0.4036, Mann–Whitney test). No significant changes were observed in the SPN (Figure 6cvi; U = 811, $p = 0.0506$, Sham: 1.545 ± 0.2263 vs. Endo: 2.333 ± 0.2861, Mann–Whitney test).

Overall, these in vivo results indicate that mice with endometriosis have enhanced nociceptive signalling into the spinal cord in response to vaginal distension.

3.5 | Mice with endometriosis display glial cell activation within the dorsal horn of the spinal cord

We then investigated if, in addition to increased peripheral mechanosensitivity, alterations occurring within the spinal cord itself contribute to the enhanced nociceptive signalling seen in mice with endometriosis. Specifically, we aimed to determine whether there was evidence of microglia and astrocyte activation within the lumbosacral areas of the spinal cord where increased numbers of pERK-IR neurons were observed.

To assess microglia activation, we performed immunostaining of LS spinal cord sections (L6-S2) from Sham mice and mice with endometriosis, with the ionized calcium-binding adaptor molecule (Iba1) (Figure 7a,b). We found that mice with endometriosis displayed a reduction in the total area covered by Iba1-positive staining across all regions of the dorsal horn (Figure 7ci; dorsal horn; U = 442, $p < 0.0001$, Sham: 15353 ± 574.1 vs. Endo: 12421 ± 706.6, SDH; U = 654, $p = 0.0128$, Sham: 2928 ± 159.6 vs. Endo: 2425 ± 169.1, DDH;

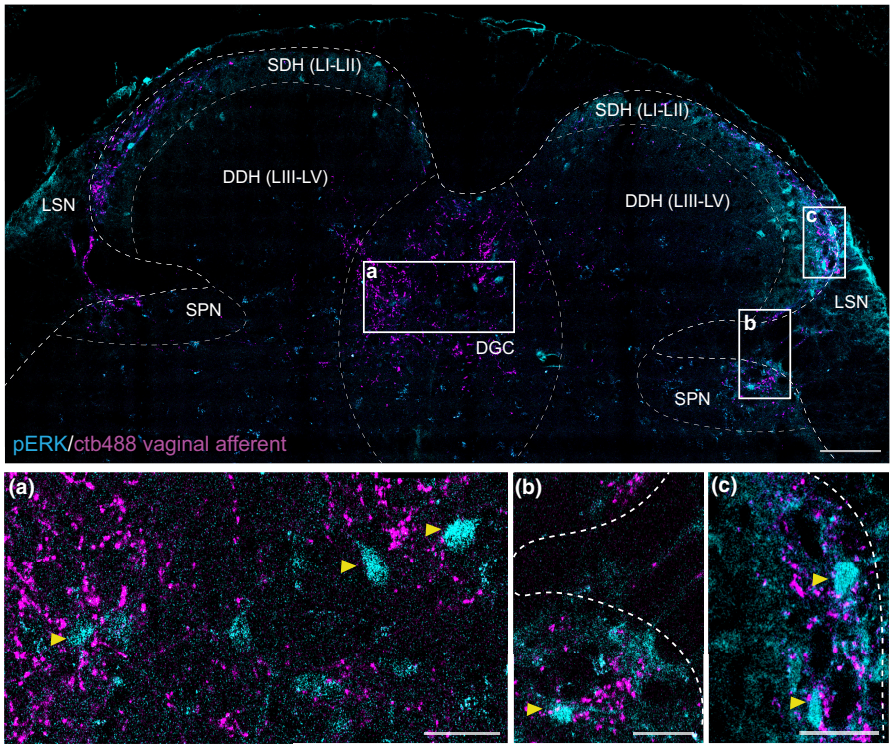

FIGURE 5 Spinal cord dorsal horn neurons activated by noxious vaginal distension are surrounded by the nerve terminals of DRG sensory neurons innervating the vagina. Representative image of a full cross-section of the lumbosacral (S1) spinal cord, showing spinal projections of vagina-innervating DRG sensory neurons (in magenta) distributed within the spinal cord of a Sham mouse. Additionally, pERK-immunoreactive (pERK-IR) neurons (in cyan) showed distribution of spinal cord dorsal horn neurons activated in response to vaginal distension (60 mm Hg). Scale bar represents 100 μm. Specific areas within the spinal cord dorsal horn cross-section (boxes a, b and c) can be seen at higher magnification in lower panels showing the (a) dorsal grey commissure (DGC), (b) sacral parasympathetic ganglia (SPN) and (c) laminae I (LI) of the superficial dorsal horn (SDH) respectively. LSN = lateral spinal nuclei. Scale bars represent 20 μm. Yellow arrows show pERK-IR neurons (in cyan) surrounded by projections labelling from the vagina (in magenta).

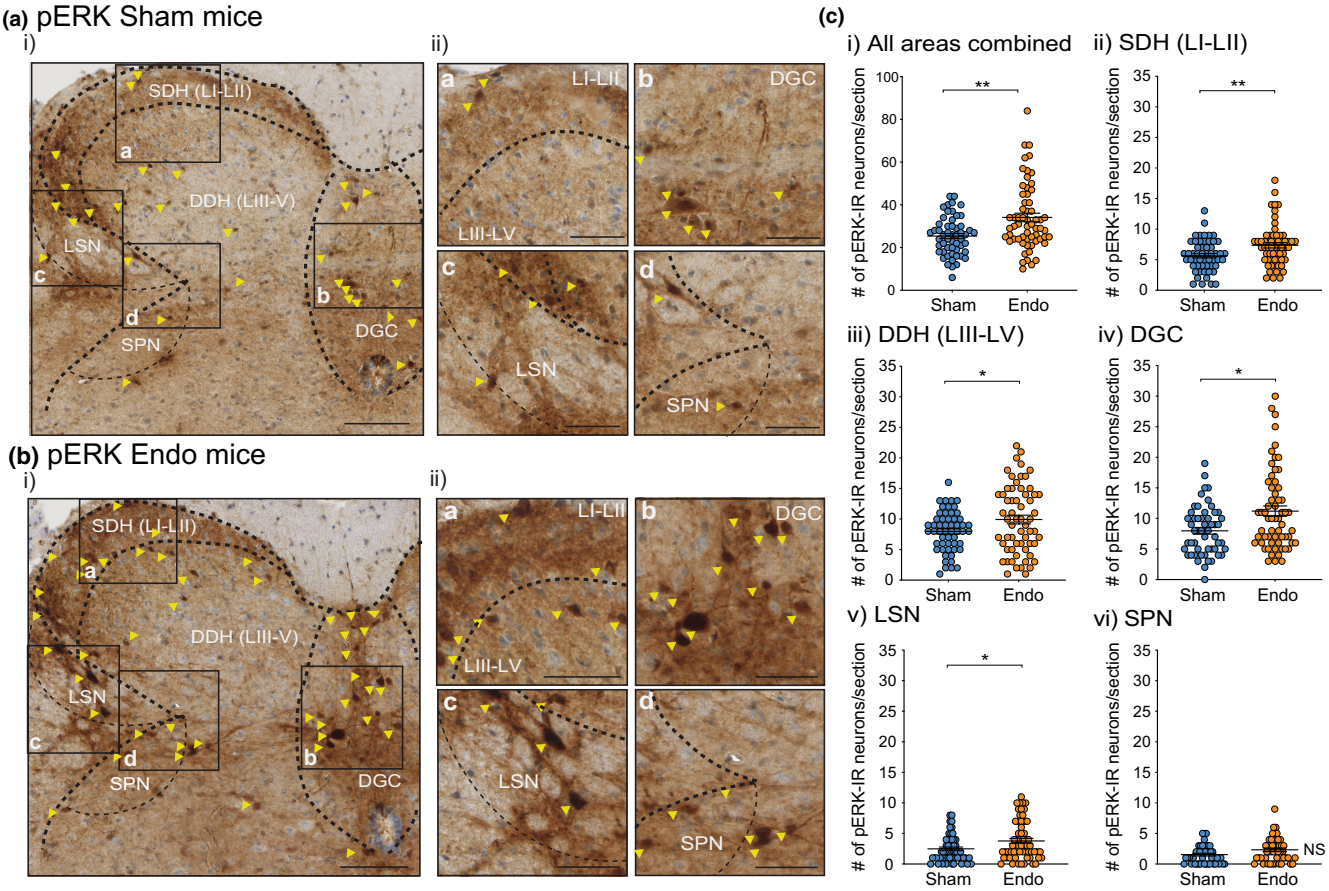

FIGURE 6 Mice with endometriosis displayed enhanced nociceptive signalling in the dorsal horn of the spinal cord in response to vaginal distension, in vivo. (a, b) pERK immunoreactivity (pERK-IR) was measured to determine activation of spinal cord dorsal horn neurons in response to noxious vaginal distension (60 mm Hg), within the lumbosacral (LS; L6-S2) spinal cord. Representative images of S1 spinal cord cross-section of (i) Sham mice and (i) Endo mice showing pERK-immunoreactive (pERK-IR) neurons (indicated by yellow arrowheads). Scale bars represent 100 μm. Specific areas (a–d) within the spinal cord cross-section (black boxes) can be seen at higher magnification in panels (a, ii) and (b, ii). Scale bars represent 20 μm. (c) Grouped data showing the number of pERK-IR neurons/section across the dorsal horn of the spinal cord. (i) Analysis of all the areas combined showed mice with endometriosis displayed a significantly increased number of pERK-IR neurons in response to vaginal distension, compared to Sham mice (**$p = 0.0022$, Mann–Whitney test). Additionally, analysis of specific areas within the spinal cord showed that, compared to Sham mice, Endo mice have significantly increased pERK-IR neurons in the (ii) superficial dorsal horn (SDH; **$p = 0.0059$, Mann–Whitney test), (iii) deep dorsal horn (DDH; *$p = 0.0279$, unpaired student's *t*-test), (iv) dorsal grey commissure (DGC; *$p = 0.0105$, Mann–Whitney test) and (v) lateral spinal nucleus (LSN; *$p = 0.0315$, Mann–Whitney test). No significant changes were observed within the (vi) sacral parasympathetic nucleus (SPN; $p = 0.0506$, Mann–Whitney test). Individual data points represent the number of pERK-IR neurons in a section of LS spinal cord, with a minimum of nine sections collected per mouse, from $N = 4$ Sham mice and $N = 5$ Endo mice. Data represent mean ± SEM. NS = Not Significant.

U = 467, $p > 0.0001$, Sham: 9692 ± 432.3 vs. Endo: 7558 ± 489.4, DGC; U = 607, $p = 0.0037$, Sham: 2675 ± 113.5 vs. Endo: 2276 ± 111.9, Mann–Whitney test). This difference was not attributed to changes in the overall area in which Iba1 immunoreactivity was quantified (Figure 7cii; dorsal horn; $t = 0.3559$, $df = 369$, $p = 0.7230$, Sham: 2503 ± 29.93 vs. Endo: 2521 ± 42.55, SDH; $t = 0.8140$, $df = 78$, $p = 0.4181$; Sham: 1338 ± 22.94 vs. Endo: 1310 ± 25.79, DDH; $t = 0.3458$, $df = 180$, $p = 0.7304$, Sham: 2161 ± 29.88 vs. Endo: 2145 ± 35.86, DGC; $t = 0.1264$, $df = 85$, $p = 0.8997$, Sham: 938 ± 15.60 vs. Endo: 940.6 ± 12.90, unpaired Student's *t*-test), or to the number of Iba1-positive cells present within each of those regions (Figure 7ciii; Dorsal horn; U = 827, $p < 0.3130$, Sham: 19.64 ± 0.7701 vs. Endo: 21.28 ± 0.9907, SDH; U = 812, $p = 0.2525$, Sham: 4.477 ± 0.3308 vs. Endo: 5.163 ± 0.3808, DDH; U = 930, $p > 0.8937$, Sham: 12.25 ± 0.5274 vs. Endo: 12.51 ± 0.7202, DGC; U = 724.5, $p = 0.0559$, Sham: 2.864 ± 0.2358 vs. Endo: 3.605 ± 0.2747, Mann–Whitney test), but rather to a reduction in the size of each Iba1-positive cell (Figure 7di; dorsal horn; U = 1 311 489, $p < 0.0211$, Sham: 142.4 ± 3.106 vs. Endo: 132.8 ± 3.115, Mann–Whitney test). Specifically, a reduction in cell size was found within the deep dorsal horn (DDH) but not the superior dorsal horn (SDH) or the dorsal grey commissure (DGC) (DDH; U = 37 430, $p = 0.0099$, Sham: 155.2 ± 4.326 vs. Endo: 140.2 ± 4.199, SDH; U = 8824, $p = 0.2669$, Sham: 113.7 ± 4.939 vs. Endo: 104.6 ± 4.610, DGC; U = 5327, $p = 0.6743$, Sham: 151.4 ± 7.504 vs. Endo: 149.0 ± 7.935, Mann–Whitney test). When comparing the size of the processes associated with each Iba1-positive cell (total

Iba-positive cell size excluding the nucleus), we saw that the changes in overall cell size were consistent with a reduction in the size of the cell's processes within the same regions of the spinal cord (Figure 7dii; dorsal horn; U = 132691, $p = 0.0387$, Sham: 108.1 ± 2.847 vs. Endo: 100.5 ± 2.904, SDH; U = 9046, $p = 0.4378$, Sham: 81.38 ± 4.446 vs. Endo: 75.32 ± 4.267, DDH; U = 37412, $p = 0.0096$, Sham: 120.5 ± 3.977 vs. Endo: 106.9 ± 3.940, DGC; U = 5400, $p = 0.8001$, Sham: 115.4 ± 6.799 vs. Endo: 115.5 ± 7.385, Mann–Whitney test). The observed changes are consistent with microglia processes shifting from a morphologically ramified state ('resting') to an intermediate ('activated') state, with retracted process and decreased arborization, indicative of microglia activation (Kettenmann et al., 2011; Nimmerjahn et al., 2005; Saijo & Glass, 2011).

Activated microglia are known to release pro-inflammatory cytokines, which subsequently activate surrounding astrocytes in a process called astrogliosis (Clark et al., 2013; Honore et al., 2000; Old & Malcangio, 2012; Scholz & Woolf, 2007; Zhou et al., 2018). We investigated whether mice with endometriosis displayed signs of increased astrocytes activation. As an indicator of astrocyte activation, we performed immunostaining of LS spinal cord sections (L6-S2), with the glial fibrillary acidic protein (GFAP, Figure 8). It has been described that most astrocytes up-regulate their cytoskeletal protein GFAP in a variety of inflammatory disorders (Sofroniew, 2014), therefore an increase in GFAP signal would be indicative of an increase in astrocyte activation. We found that mice with endometriosis displayed a significant increase in GFAP staining in all dorsal horn areas of the LS spinal (Figure 8ci; dorsal horn: $t = 5.719$, $df = 95$, $p \leq 0.0001$, Sham: 30873 ± 1062 vs. Endo: 43137 ± 1876, unpaired Student's *t*-test). Sub-analysis of individual areas within the spinal cord showed a significant increase in GFAP staining within each area of the dorsal horn examined (Figure 8ci; SDH: $t = 4.764$, $df = 95$, $p \leq 0.0001$, Sham: 11020 ± 475.5 vs. Endo: 15586 ± 838.1, unpaired Student's *t*-test; DDH: U = 5174, $p \leq 0.0001$, Sham: 12732 ± 548.9 vs. Endo 19031 ± 979.0, Mann–Whitney test; and DGC: $t = 4.403$, $df = 95$, $p \leq 0.0001$, Sham: 6549 ± 218.7 vs. Endo: 8135 ± 287.6, unpaired Student's *t*-test). Comparison of the perimeter area in which GFAP immunoreactivity was quantified showed similar areas of dorsal horn was analysed between experimental groups (Figure 8cii; dorsal horn: $t = 1.890$, $df = 82$, $p = 0.0623$, Sham: 2499 ± 40.97 vs. Endo: 2616 ± 46.1, unpaired Student's *t*-test; SDH: $t = 0.6283$, $df = 76$, $p = 0.5317$, Sham: 1309 ± 22.82 vs. Endo 1333 ± 30.58, unpaired Student's *t*-test, DDH: $t = 0.9414$, $df = 84$, $p = 0.3492$, Sham: 2184 ± 33.43 vs. Endo 2235 ± 42.19, unpaired Student's *t*-test; and DGC: U = 1018, $p = 0.2571$, Sham: 910.9 ± 16.07 vs. Endo: 925.3 ± 14.27, Mann–Whitney test). We found the increased staining in GFAP observed in the spinal cord of mice with endometriosis was caused by an increase in the total number of GFAP-positive cells across the dorsal horn of the spinal cord, compared to Sham mice (Figure 8ciii; dorsal horn: $t = 4.891$, $df = 93$, $p < 0.0001$, Sham: 30.24 ± 1.096 vs. Endo: 38.83 ± 1.384, unpaired Student's *t*-test; SDH: $t = 1.307$, $df = 93$, $p = 0.1946$, Sham: 9.959 ± 0.4555 vs. Endo 10.87 ± 0.5308, unpaired Student's *t*-test, DDH: $t = 5.079$, $df = 93$, $p < 0.0001$, Sham: 12.80 ± 0.6151 vs. Endo 18.15 ± 0.8692, unpaired Student's *t*-test; and DGC: U = 688.5, $p = 0.0009$, Sham: 7.531 ± 0.4207 vs. Endo: 9.826 ± 0.4898, Mann–Whitney test). Overall, our findings indicate that mice with endometriosis developed signs of astrogliosis within the dorsal horn of the LS spinal cord.

3.6 | Mice with endometriosis displayed sensitization of nociceptive neuronal circuits within the dorsal horn of the spinal cord

We then investigated whether the increased sensory input and/or neuroinflammation evident in the spinal cord of endometriosis mice may have led to alterations of neuronal circuits within the same LS regions of the spinal cord. For this, we quantified the levels of neurokinin 1 receptor (NK1r) within the LS spinal cord dorsal horn sections collected from Sham and Endo mice (Figure 9). Up-regulation of spinal NK1r has been shown in numerous visceral hyperalgesia models that involve spinal microglia activation (Bradesi et al., 2009; Palotai et al., 2018).

We found that NK1r immunoreactivity was observed within the superficial dorsal horn (SDH; LI-II), the dorsal grey commissure (DGC) and the deep dorsal horn (DDH; LIII-V) in both Sham (Figure 9a) and Endo (Figure 9b) mice. The area covered by NK1r immunoreactivity was significantly increased in Endo compared to Sham mice (Figure 9ci; dorsal horn: $t = 3.828$, $df = 40$, $p = 0.0004$, Sham: 13241 ± 1520 vs. Endo: 22681 ± 1855; SDH: $t = 1.445$, $df = 39$, $p = 0.1563$, Sham: 875.2 ± 139.3 vs. Endo: 1285 ± 234.4; DDH: $t = 3.208$, $df = 40$, $p = 0.0026$, Sham: 2129 ± 266.1 vs. Endo 4081 ± 506.5; and DGC: $t = 3.403$, $df = 40$, $p = 0.0015$, Sham: 8782 ± 1080 vs. Endo: 14274 ± 1164; unpaired Student's *t*-test). This increase in NK1r immunoreactivity occurred specifically within the DDH and the DGC regions of the spinal cord (Figure 9ci). Comparison of the perimeter area in which NK1r immunoreactivity was quantified showed similar areas of dorsal horn were analysed between experimental groups (Figure 9cii; dorsal horn: $t = 0.8218$, $df = 40$, $p = 0.4616$; SDH: $t = 0.7661$, $p = 0.4481$, DDH: $t = 0.02448$, $df = 40$, $p = 0.9806$ and DGC: $t = 0.1314$, $df = 40$, $p = 0.8961$, unpaired Student's *t*-test).

Overall, the data presented here show that mice with endometriosis developed an increase in nociceptive signals arising from the female reproductive tract, specifically via pelvic nerves relayed into specific regions of the LS spinal cord. Moreover, the same areas of the LS spinal cord receiving increased nociceptive input developed signs of neuroinflammation, with indications of both microgliosis and astrogliosis. Finally, as revealed by an increase in NK1r immunoreactivity, we present evidence suggesting these alterations may induce changes within specific neuronal circuits within the spinal cord.

4 | DISCUSSION

In the current study, we provide experimental evidence showing well-defined peripheral and central neuroplasticity in a mouse

model of endometriosis. We demonstrate that primary pelvic sensory afferents innervating the vagina of mice with endometriosis developed hypersensitivity to mechanical stimuli. In addition, we show that the sensory input from the vagina to the CNS is augmented in endometriosis. Moreover, we identify alterations in glial cells, astrocytes and neuronal circuitry within the spinal cord that may explain the increased sensitivity to pain occurring in endometriosis.

Increased pain sensitivity is a cardinal feature seen in both pre-clinical animal models and women with endometriosis (As-Sanie et al., 2013; Berkley et al., 2001; Berkley et al., 2005; Castro et al., 2021; Maddern et al., 2020; McKinnon et al., 2015; Morotti et al., 2014). In this study, we demonstrate that pelvic afferents innervating the vagina from mice with endometriosis are hypersensitive to an array of mechanical stimuli. In addition, these sensory afferents of mice with endometriosis responded earlier, responded for a longer period of time and fired more action potentials, indicating a 'stronger' nociceptive input is being sent to the CNS. Previous studies have shown that sensory afferents innervating the colon and the bladder become hypersensitive to mechanical stimuli in mouse models of irritable bowel syndrome (IBS) (13–17) and interstitial cystitis/bladder pain syndrome (IC/BPS) (17–19). The present study provides evidence showing pelvic afferents innervating the vagina develop mechanical hypersensitivity in endometriosis. Moreover, it contributes to the mechanistical understanding of previous findings showing rodents with endometriosis displayed vaginal hyperalgesia, as initially reported by Berkley (Berkley et al., 2007), and later as described in similar animal models of endometriosis such as the one used in this study (Castro et al., 2021).

In addition to the pelvic nerve, we also examined the mechanosensory properties of pudendal nerves innervating the vagina. Our results showed that unlike afferents within the pelvic nerve, which displayed polymodal responses, primary afferents from the pudendal nerve were more selective to the type of mechanical stimuli to which they responded, with only half of afferents responding to circular stretch and two-thirds responding to fine stroking of the vaginal surface. In addition, and in contrast to that identified in the pelvic nerve, we found that sensory afferents from the pudendal nerve of mice with endometriosis did not develop mechanical hypersensitivity. The difference in mechanosensory properties between these sensory afferents seen in our model may be caused by placement of endometriosis lesions. The pudendal nerve predominantly innervates the lower region of the vagina and external genitalia. In this model, lesions are restricted to the intestinal mesentery and uterus rather than lower regions of the female reproductive tract, which may limit any effect on the pudendal nerve. While not as common, in rare cases, endometriotic lesions are known to infiltrate the lower portion of the vagina, affect the pudendal nerve and induce pudendal neuralgia symptoms (Ceccaroni et al., 2010; Maillard et al., 2021). It may be the case that if lesions were placed towards the lower portion of the vagina, altered afferent sensitivity may be apparent.

Studies in animal models of IBS, where chronic pelvic pain is also a major symptom, revealed that afferent hypersensitivity is observed ex vivo and is often accompanied by hyperexcitability of cultured colon- and bladder-innervating neurons, in vitro (Castro et al., 2018; Grundy, Harrington, et al., 2018; Malykhina et al., 2006; Osteen et al., 2016). Interestingly, our in vitro patch clamp experiments showed that the excitability of cultured vagina-innervating neurons was similar in Sham mice and mice with endometriosis. Whether this is because neurons are cultured in an isolated/artificial environment (in the absence of inflammatory mediators and other endometriosis-related factors co-existing in the local environment) is yet to be determined. Moreover, patch clamp experiments were performed on cultured DRG isolated from the lumbosacral region (L6-S1), which is known to contain neurons supplying both the pelvic and the pudendal innervation. Interestingly, we show that vagina-innervating afferents via the pudendal nerve, which are spatially separated from the endometriotic lesion site, failed to develop hypersensitivity to mechanical stimuli. This could in part explain the results obtained in the patch clamp recordings, where a heterogenous population of retrogradely traced DRG neurons was used.

We have previously shown that noxious distension of the vagina evoked activation of dorsal horn neurons within the LS

FIGURE 7 Mice with endometriosis developed microgliosis within the dorsal horn of the spinal cord. Ionized calcium-binding adaptor molecule (Iba1) staining was performed to determine microglia activation within the (LS; L6-S2) spinal cord. Representative images of Iba1 immunoreactivity in LS (S1) spinal cord cross-section of (a) Sham mice and (b) Endo mice. Scale bars represent 100 μm. Specific areas within the spinal cord cross-section (black inset boxes) can be seen at higher magnification in panels (a–c). Scale bars represent 50 μm. (c, i) Grouped data showing the total area covered by IbA1 staining in each of the dorsal horn areas analysed is significantly reduced in mice with endometriosis, compared to Sham mice (dorsal horn; $^{****}p < 0.0001$, SDH; $^{*}p = 0.0128$, DDH; $^{****}p < 0.0001$, DGC; $^{**}p = 0.0037$, Mann–Whitney test). (c, ii) Comparison of the perimeter area in which Iba1 immunoreactivity was quantified confirmed similar areas were analysed between experimental groups (dorsal horn; $p = 0.7230$, SDH; $p = 0.4181$, DDH; $p = 0.7304$, DGC; $p = 0.8997$, unpaired Student's *t*-test). (c, iii) The number of Iba1-positive cells counted within each of those regions was similar between Sham and Endo mice (dorsal horn; $p = 0.3130$, SDH; $p = 0.2524$, DDH; $p = 0.8937$, DGC; $p = 0.0559$, Mann–Whitney test). (d, i) The area occupied by each individual Iba1-positive cell was significantly lower across the dorsal horn (dorsal horn; $^{*}p = 0.0211$, Mann–Whitney test), with a significant reduction observed specifically within the deep dorsal horn (DDH; $^{**}p = 0.0099$, Mann–Whitney test), with no significant changes observed within the SDH ($p = 0.2669$, Mann–Whitney test) or DGC ($p = 0.6743$, Mann–Whitney test). (d, ii) Grouped data showing the total area covered by cellular processes of individual cells are significantly reduced within the dorsal horn of the spinal cord of mice with endometriosis compared to Sham mice ($^{*}p = 0.0387$, unpaired Student's *t*-test), with more pronounced differences observed within the deep dorsal horn (DDH; $^{**}p = 0.0096$), with no significant changes observed within the SDH ($p = 0.4378$, Mann–Whitney test) or the DGC ($p = 0.8001$, Mann–Whitney test). Data presented as mean ± SEM with dots showing individual spinal cord sections from $N = 6$ mice/experimental group, from a minimum of seven sections per mouse. NS = Not Significant.

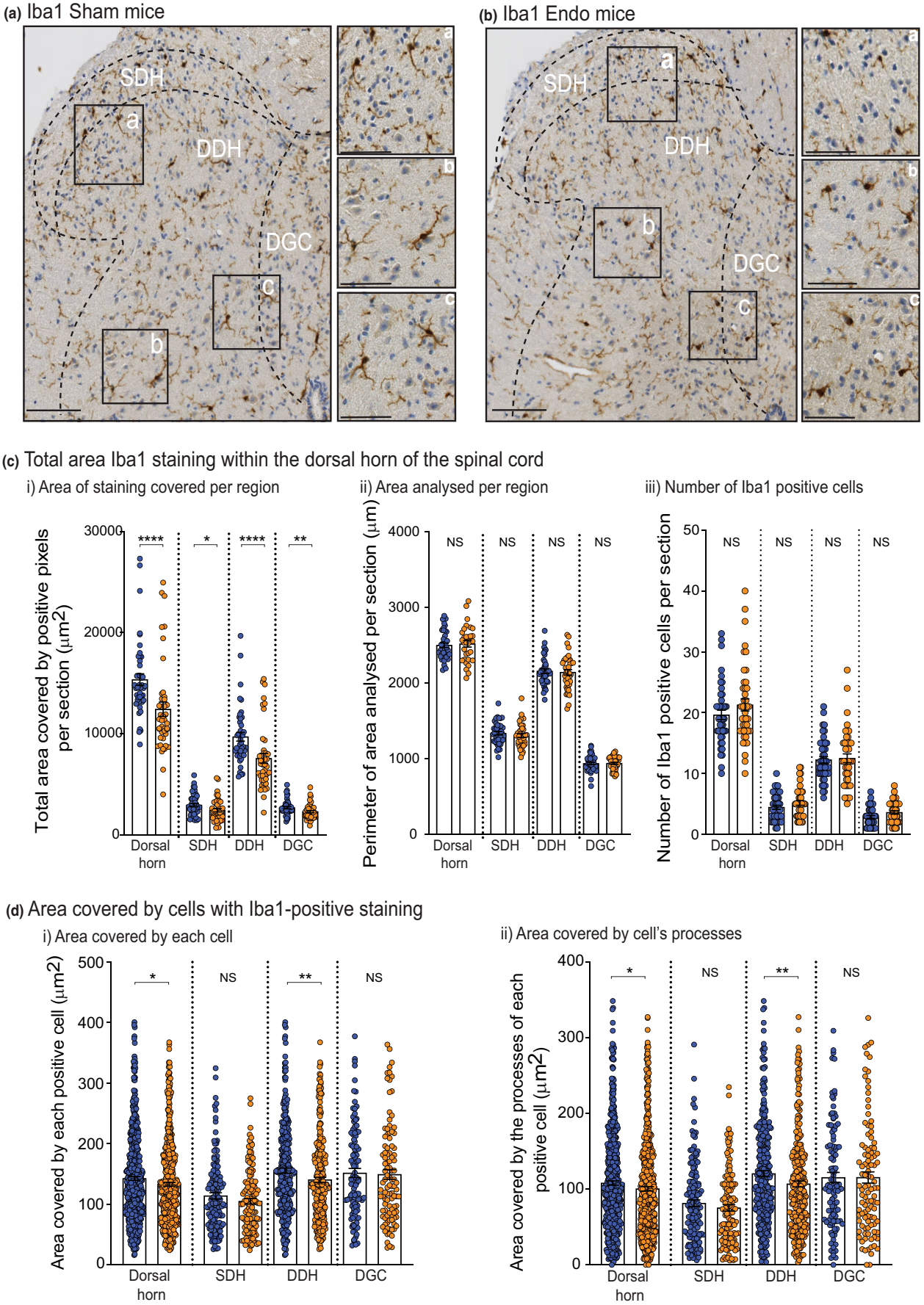

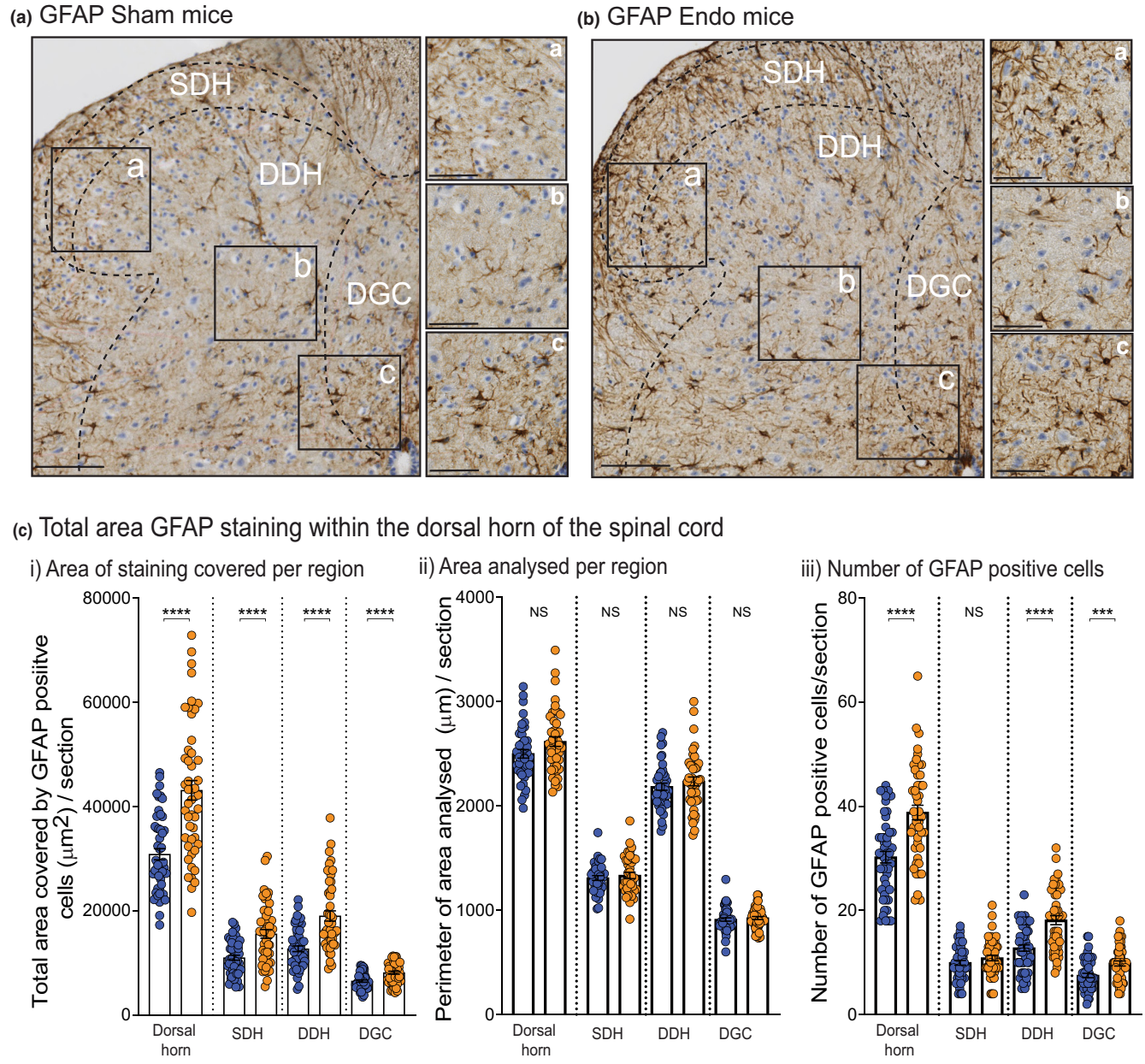

FIGURE 8 Mice with endometriosis developed astrogliosis within the dorsal horn of the spinal cord. Glial fibrillary acidic protein (GFAP) staining was performed to determine astrocyte activation within the lumbosacral (LS; L6-S2) spinal cord. Representative images of GFAP immunoreactivity in LS (S1) spinal cord cross-section of (a) Sham mice and (b) Endo mice. Scale bars represent 100 µm. Specific areas within the spinal cord cross-section (black boxes) can be seen at higher magnification within inset panels (a–c). Scale bars represent 50 µm. (c, i) Grouped data showing mice with endometriosis (orange symbols) displayed an increase in the overall area covered by GFAP staining in each of the regions of the spinal cord analysed, compared to Sham mice (dorsal horn, SDH and DGC; $^{****}p < 0.0001$, unpaired Student's *t*-test and DDH; $^{****}p < 0.0001$, Mann–Whitney test). (c, ii) Comparison of the perimeter area in which GFAP immunoreactivity was quantified confirmed similar areas were analysed between experimental groups (dorsal horn; $p = 0.0623$, SDH; $p = 0.5317$, DDH; $p = 0.3492$; unpaired Student's *t*-test and DGC; $p = 0.2571$, Mann–Whitney test). (c, iii) Grouped data showing mice with endometriosis displayed a significant increase in the number of GFAP-positive cells in all dorsal horn areas combined, compared to Sham mice (blue symbols, dorsal horn, $^{****}p < 0.0001$, unpaired Student's *t*-test). Analysis of specific areas within the spinal cord showed GFA-positive cells were significantly increased within the deep dorsal horn (DDH; $^{****}p < 0.0001$, unpaired Student's *t*-test) and dorsal grey commissure (DGC; $^{***}p = 0.0009$, Mann–Whitney test), but not the SDH ($p = 0.1946$, unpaired Student's *t*-test). Data presented as mean ± SEM with dots showing in individual spinal cord sections from $N = 6$ mice/experimental group, from a minimum of eight sections per mouse. NS = Not Significant.

spinal cord of healthy naïve mice, in vivo (Castro et al., 2020). In the present study, we investigated whether this nociceptive signal was enhanced in mice with endometriosis. We found that noxious distension of the vagina indeed evoked enhanced activation of dorsal horn neurons within the spinal cord of mice with endometriosis when compared to Sham mice. We also found dorsal horn neurons

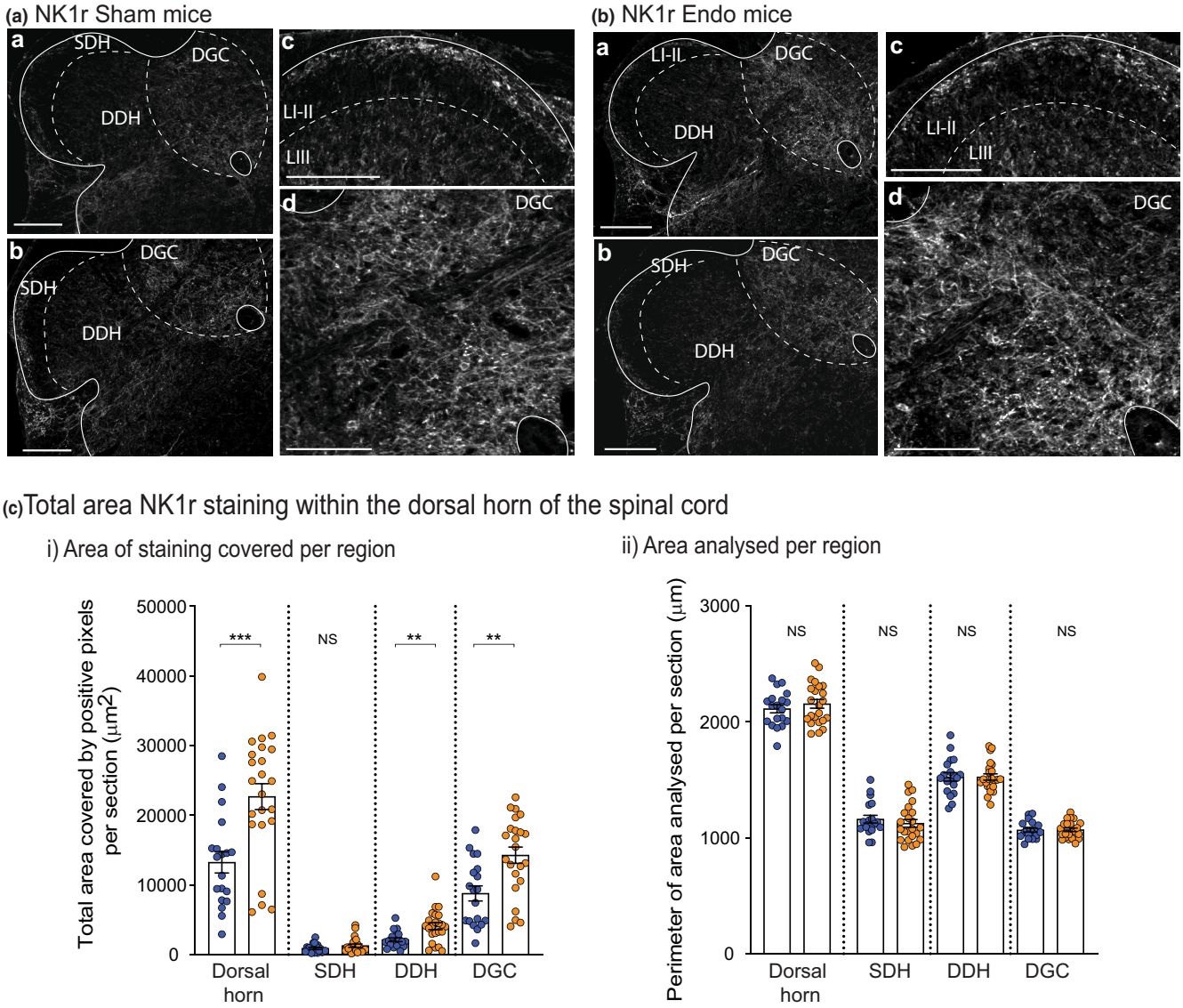

FIGURE 9 Mice with endometriosis displayed sensitization of neuronal circuits within the dorsal horn of the LS spinal cord. Neurokinin 1 receptor (NK1r) immunolabelling was performed to examine changes occurring within specific dorsal horn circuits associated with endometriosis. Representative images of NK1r immunoreactivity in cross-sections of lumbosacral (LS; L6-S2) spinal cord dorsal horn of (a) Sham and (b) Endo mice. High-magnification images, taken from other cross-sections, are shown in panels (c) and (d). Scale bars represent 100 μm. Dashed lines show the ventral border of Lamina II (LII) and the lateral borders of the dorsal grey commissure (DGC). Dense NK1r immunoreactivity was observed in the superficial dorsal horn lamina I (LI), the DGC and in the sacral parasympathetic nucleus (SPN) and to a lesser degree in the deep dorsal horn (LIII-V). (c, i) Grouped data showing mice with endometriosis (orange symbols) displayed a significant increase in NK1r immunoreactivity in all dorsal horn areas combined, compared to Sham mice (Dorsal horn, $^{***}p = 0.0004$, unpaired Student's *t*-test). Analysis of specific areas within the spinal cord showed a significant increase in NK1r immunoreactivity within the deep dorsal horn (DDH, $^{**}p = 0.0026$, unpaired Student's *t*-test) and the dorsal grey commissure (DGC, $^{**}p = 0.0015$, unpaired Student's *t*-test), but not within the superficial dorsal horn (SDH, $p = 0.1563$, unpaired Student's *t*-test). (c, ii) Comparison of the perimeter area in which NK1r immunoreactivity was quantified confirmed similar areas were analysed between experimental groups (dorsal horn; $p = 0.4616$, SDH; $p = 0.4481$, DDH; $p = 0.9806$, DGC; $p = 0.8961$, unpaired Student's *t*-test). Data presented as mean ± SEM with individual data points representing spinal cord sections, $n = 5$ sections/mouse from $N = 5$ mice/experimental group. NS = Not Significant.

activated by vaginal distension were distributed around the projections of vagina-innervating sensory neurons within the spinal cord. Moreover, specific regions of the spinal cord, where neuronal activation occurred, are known to be involved in integrating nociceptive input from pelvic organs affected in chronic pelvic pain conditions such as IBS and IC/BPS (Castro et al., 2019, 2020; Grundy, Erickson, et al., 2018; Harrington et al., 2012, 2019). This is important as in addition to vaginal hyperalgesia, it is known that both mice (Castro et al., 2021; Maddern et al., 2021) and women with endometriosis (Arnold et al., 2012; Berkley et al., 2005; Maddern et al., 2020) can develop colonic and bladder hyperalgesia, suggesting increased pain processing within the CNS is associated with this disorder.

In this study, we also investigated whether changes occurring within the regions of the spinal cord receiving increased peripheral nociceptive input would amplify neural signalling within the CNS, which ultimately contributes to chronic pain in a process known as central sensitization (Latremoliere & Woolf, 2009). The contribution of central glial cells to the pathogenesis of pain induction and maintenance has been identified in diverse chronic pelvic pain disorders (Peng et al., 2016; Taves et al., 2013; Tsuda, 2016). Under normal conditions, microglia are the only immunocompetent cells within the nervous system (Deleo & Yezierski, 2001; Watkins et al., 2001). After peripheral injury, spinal cord microglial cells undergo activation (microgliosis), characterized by a change in their shape, function and chemical expression (Raghavendra et al., 2004; Saijo & Glass, 2011; Vega-Avelaira et al., 2009; Zhou et al., 2018). These changes lead to the synthesis and release of cytokines, contributing to the initiation and maintenance of CPP (Honore et al., 2000; Raghavendra et al., 2004; Vega-Avelaira et al., 2009; Zhou et al., 2018).

We examined the expression of the ionized calcium-binding adapter molecule 1 (Iba-1), a microglia/macrophage-specific marker (Imai et al., 1996; Ito et al., 1998), and found an overall reduction in Iba1 staining within the spinal cord of mice with endometriosis. These results somewhat conflict with previous studies which have shown an increase in Iba1-positive staining (indicative of microglia proliferation) in inflammatory disorders, including endometriosis (Dodds et al., 2019; Ito et al., 1998; Liu et al., 2018). However, this disparity may be explained by the timeframe in which Iba1 has been visualized/quantified, relative to the onset of the inflammatory event. For example, microglia Iba1-positive staining has been reported to remain unchanged in late-onset inflammatory disorders such as Alzheimer's disease (Hopperton et al., 2018). Similarly, in a rat model of neuroinflammation, elevated levels of Iba1 staining are observed at 2 weeks following microbial enzyme injection but return to control levels by 10 weeks following this inflammatory insult (Leon-Rodriguez et al., 2022). In line with this, the time-dependent changes in microglia activity may explain why the increase in Iba1 staining was previously associated with the early development of endometriosis (3 weeks following endometriosis induction) (Dodds et al., 2019; Liu et al., 2018), which were not seen in our study at 8–10 weeks post-endometriosis induction. Interestingly, we found that the endometriosis-associated reduction in spinal Iba1 staining occurred without a change in the total number of Iba1-positive cells but was rather explained by a reduction in the overall size of microglia, driven by a retraction of their cellular processes. Our results, therefore, align with what has been seen in other chronic inflammatory disorders, with the normal ramified morphology of microglia cells changing to an amoeboid morphology, identified by highly retracted processes, following chronic disease progression (Hanisch & Kettenmann, 2007).

Activated microglia subsequently activate surrounding astrocytes (astrogliosis) in a cascade that initiates the prolonged release of inflammatory mediators, able to sensitize adjacent centrally projecting neurons, inducing central sensitization and ultimately chronic pain (Clark et al., 2013; Honore et al., 2000; Old & Malcangio, 2012; Scholz & Woolf, 2007; Zhou et al., 2018). To investigate astrogliosis, we quantified an increase in glial fibrillary acidic protein (GFAP) immunoreactivity, as previously described (Eng & Ghirnikar, 1994). Astrogliosis has previously been suggested to occur in endometriosis, with changes seen in GFAP staining within the thoracolumbar (T13-L1) but not the lumbosacral (L6-S1) region of the spinal cord at 3 weeks post-endometriosis induction (Dodds et al., 2019). In contrast, we have shown astrogliosis development in the lumbosacral region of the spinal cord (displayed by both an increase in GFAP staining and the number of GFAP-positive cells), within the longer development of 8–10 weeks following endometriosis induction. Importantly, the lumbosacral region of the spinal cord plays a crucial role in processing nociceptive information from the vagina (also shown in this study), suggesting that neuroinflammation developed within this region contributes to vagina hyperalgesia and CPP in endometriosis.

Taken together, our results support the concept of a time-dependent role of both microgliosis and astrogliosis across the stages of inflammatory disease development. This differentiation is important as endometriosis is a chronic inflammatory disease, the centrally mediated mechanisms that may drive central sensitization and chronic pain seen in endometriosis may be different from those previously described at earlier time points. To further understand the differential stages of the disease, it would be important to look at the changes over various time points in our model development, however, this was out of scope of the current study.

Quantitative sensory testing and magnetic resonance imaging (MRI) studies suggest that women with endometriosis develop central sensitization (As-Sanie et al., 2012, 2013; Grundstrom et al., 2019). The development of central sensitization has also been suggested using animals models demonstrated by altered behaviour accompanied by abnormal expression of genes within the brain of mice with endometriosis (Greaves et al., 2017; Li et al., 2018); together with glial changes within the spinal cord in a mouse model of endometriosis (Dodds et al., 2016). In the present study, we show that mice with endometriosis displayed an increase in immunoreactivity for neurokinin type 1 receptor (NK1r) within the same regions of the LS spinal cord where the enhanced nociceptive input occurred. This increase in NK1r immunoreactivity may be linked to the neuroinflammation evident within the spinal cord (particularly within DDH and the DGC, where we saw overlapping changes), or be driven by different neuronal processes occurring in parallel or at slightly different time points (i.e. activity-dependent sensitization). It is well known, from other chronic pain disorders, that NK1r up-regulation within dorsal horn neurons induces their sensitization (Gautam et al., 2016) and long-term potentiation of the first-order synapses of nociceptors (Ikeda et al., 2003; Liu & Sandkuhler, 1998). Further experiments are required to determine the direct link between increased NK1r immunoreactivity and the neuroinflammation evident. However, an inflammatory environment involving interleukin 1β (which is known to be up-regulated within the peritoneal fluid in this mouse model of endometriosis (Castro et al., 2021)) can also increase NK1 receptor expression within glial cells, potentiating the response to the neuropeptide, substance P. This in turn facilitates

the release of ATP and proinflammatory cytokines from surrounding astrocytes, and ultimately contributes to the central sensitization observed in several inflammatory disorders (Dodds et al., 2016).

In summary, our study shows key peripheral and central neuroplasticity associated with the development of endometriosis. These findings support the hypothesis that sensitization of sensory afferent pathways occurs at peripheral and central sites and contributes to the initiation and maintenance of endometriosis-associated CPP. Importantly, these findings provide the platform for the investigation and development of novel analgesic treatments targeted to relieve CPP associated with endometriosis.

AUTHOR CONTRIBUTIONS

J.C, A.M.H, J.M, A.E and S.M.B contributed with the experimental design. J.C, A.M.H, J.M and A.E performed the experiments described in this paper. J.C, A.M.H and J.M made the figures. J.C wrote the manuscript. All authors contributed to manuscript's proofreading.

ACKNOWLEDGEMENTS

We thank Dr. Luke Grundy for his intellectual input in the early stages of the study and for providing feedback on the first manuscript's draft. J.C is funded by a National Health and Medical Research Council (NHMRC) of Australia Ideas Grant (APP1181448). A.M.H received funding through the Australian Research Council (ARC) Discovery Early Career Research Award (DE130100223). J.M is funded by The Hospital Research Foundation (THRF) PhD Scholarship (SAPhD000242018) Australia. S.M.B is funded by an NHMRC Investigator Leadership Grant (APP2008727) and an NHMRC Development Grant (APP2014250). A.M.H and S.M.B received funding via an ARC Discovery Project (DP180101395). A.M.H and S.M.B received funding via an ARC Discovery Project (DP220101269). Open access publishing facilitated by Flinders University, as part of the Wiley - Flinders University agreement via the Council of Australian University Librarians.

CONFLICT OF INTEREST STATEMENT

Stuart Brierley is a Guest Editor for the special issue "Pain". The rest of the authors have declared no conflict of interest.

PEER REVIEW

The peer review history for this article is available at https://www.webofscience.com/api/gateway/wos/peer-review/10.1111/jnc.15843.

DATA AVAILABILITY STATEMENT

The data that support the findings of this study are available from the corresponding author upon reasonable request.

PRE-REGISTRATION

This study was not pre-registered.

PREVIOUS PRESENTATION OF RESEARCH

This study has not been presented elsewhere.

ORCID

Joel Castro https://orcid.org/0000-0002-5781-2224

REFERENCES

Abbott, J., Hawe, J., Hunter, D., Holmes, M., Finn, P., & Garry, R. (2004). Laparoscopic excision of endometriosis: A randomized, placebo-controlled trial. *Fertility and Sterility*, *82*, 878–884.

Adaes, S., Almeida, L., Potes, C. S., Ferreira, A. R., Castro-Lopes, J. M., Ferreira-Gomes, J., & Neto, F. L. (2017). Glial activation in the collagenase model of nociception associated with osteoarthritis. *Molecular Pain*, *13*, 1744806916688219.

Arnold, J., Barcena De Arellano, M. L., Ruster, C., Vercellino, G. F., Chiantera, V., Schneider, A., & Mechsner, S. (2012). Imbalance between sympathetic and sensory innervation in peritoneal endometriosis. *Brain, Behavior, and Immunity*, *26*, 132–141.

Asante, A., & Taylor, R. N. (2011). Endometriosis: The role of neuroangiogenesis. *Annual Review of Physiology*, *73*, 163–182.

As-Sanie, S., Harris, R. E., Harte, S. E., Tu, F. F., Neshewat, G., & Clauw, D. J. (2013). Increased pressure pain sensitivity in women with chronic pelvic pain. *Obstetrics and Gynecology*, *122*, 1047–1055.

As-Sanie, S., Harris, R. E., Napadow, V., Kim, J., Neshewat, G., Kairys, A., Williams, D., Clauw, D. J., & Schmidt-Wilcke, T. (2012). Changes in regional gray matter volume in women with chronic pelvic pain: A voxel-based morphometry study. *Pain*, *153*, 1006–1014.

Bellono, N. W., Bayrer, J. R., Leitch, D. B., Castro, J., Zhang, C., O'donnell, T. A., Brierley, S. M., Ingraham, H. A., & Julius, D. (2017). Enterochromaffin cells are gut Chemosensors that couple to sensory neural pathways. *Cell*, *170*(185–198), e16.

Berkley, K. J. (2005). A life of pelvic pain. *Physiology & Behavior*, *86*, 272–280.

Berkley, K. J., Cason, A., Jacobs, H., Bradshaw, H., & Wood, E. (2001). Vaginal hyperalgesia in a rat model of endometriosis. *Neuroscience Letters*, *306*, 185–188.

Berkley, K. J., Hotta, H., Robbins, A., & Sato, Y. (1990). Functional properties of afferent fibers supplying reproductive and other pelvic organs in pelvic nerve of female rat. *Journal of Neurophysiology*, *63*, 256–272.

Berkley, K. J., Hubscher, C. H., & Wall, P. D. (1993). Neuronal responses to stimulation of the cervix, uterus, colon, and skin in the rat spinal cord. *Journal of Neurophysiology*, *69*, 545–556.

Berkley, K. J., Mcallister, S. L., Accius, B. E., & Winnard, K. P. (2007). Endometriosis-induced vaginal hyperalgesia in the rat: Effect of estropause, ovariectomy, and estradiol replacement. *Pain*, *132*(Suppl 1), S150–S159.

Berkley, K. J., Rapkin, A. J., & Papka, R. E. (2005). The pains of endometriosis. *Science*, *308*, 1587–1589.

Berkley, K. J., Robbins, A., & Sato, Y. (1993). Functional differences between afferent fibers in the hypogastric and pelvic nerves innervating female reproductive organs in the rat. *Journal of Neurophysiology*, *69*, 533–544.

Bradesi, S., Svensson, C. I., Steinauer, J., Pothoulakis, C., Yaksh, T. L., & Mayer, E. A. (2009). Role of spinal microglia in visceral hyperalgesia and NK1R up-regulation in a rat model of chronic stress. *Gastroenterology*, *136*(1339–48), e1–e2.

Brawn, J., Morotti, M., Zondervan, K. T., Becker, C. M., & Vincent, K. (2014). Central changes associated with chronic pelvic pain and endometriosis. *Human Reproduction Update*, *20*, 737–747.

Brierley, S. M., Castro, J., Harrington, A. M., Hughes, P. A., Page, A. J., Rychkov, G. Y., & Blackshaw, L. A. (2011). TRPA1 contributes to specific mechanically activated currents and sensory neuron mechanical hypersensitivity. *The Journal of Physiology*, *589*, 3575–3593.

Brierley, S. M., & Linden, D. R. (2014). Neuroplasticity and dysfunction after gastrointestinal inflammation. *Nature Reviews. Gastroenterology & Hepatology*, *11*, 611–627.

Burns, K. A., Rodriguez, K. F., Hewitt, S. C., Janardhan, K. S., Young, S. L., & Korach, K. S. (2012). Role of estrogen receptor signaling required for endometriosis-like lesion establishment in a mouse model. *Endocrinology*, *153*, 3960–3971.

Castro, J., Garcia-Caraballo, S., Maddern, J., Schober, G., Lumsden, A., Harrington, A., Schmiel, S., Lindstrom, B., Adams, J., & Brierley, S. M. (2022). Olorinab (APD371), a peripherally acting, highly selective, full agonist of the cannabinoid receptor 2, reduces colitis-induced acute and chronic visceral hypersensitivity in rodents. *Pain*, *163*, e72–e86.

Castro, J., Grundy, L., Deiteren, A., Harrington, A. M., O'donnell, T., Maddern, J., Moore, J., Garcia-Caraballo, S., Rychkov, G. Y., Yu, R., Kaas, Q., Craik, D. J., Adams, D. J., & Brierley, S. M. (2018). Cyclic analogues of alpha-conotoxin Vc1.1 inhibit colonic nociceptors and provide analgesia in a mouse model of chronic abdominal pain. *British Journal of Pharmacology*, *175*, 2384–2398.

Castro, J., Harrington, A. M., Garcia-Caraballo, S., Maddern, J., Grundy, L., Zhang, J., Page, G., Miller, P. E., Craik, D. J., Adams, D. J., & Brierley, S. M. (2017). Alpha-conotoxin Vc1.1 inhibits human dorsal root ganglion neuroexcitability and mouse colonic nociception via GABAB receptors. *Gut*, *66*, 1083–1094.

Castro, J., Harrington, A. M., Hughes, P. A., Martin, C. M., Ge, P., Shea, C. M., Jin, H., Jacobson, S., Hannig, G., Mann, E., Cohen, M. B., Macdougall, J. E., Lavins, B. J., Kurtz, C. B., Silos-Santiago, I., Johnston, J. M., Currie, M. G., Blackshaw, L. A., & Brierley, S. M. (2013). Linaclotide inhibits colonic nociceptors and relieves abdominal pain via guanylate cyclase-C and extracellular cyclic guanosine 3′,5′-monophosphate. *Gastroenterology*, *145*(1334–46), e1–e11.

Castro, J., Harrington, A. M., Lieu, T., Garcia-Caraballo, S., Maddern, J., Schober, G., O'donnell, T., Grundy, L., Lumsden, A. L., Miller, P., Ghetti, A., Steinhoff, M. S., Poole, D. P., Dong, X., Chang, L., Bunnett, N. W., & Brierley, S. M. (2019). Activation of pruritogenic TGR5, MrgprA3, and MrgprC11 on colon-innervating afferents induces visceral hypersensitivity. *JCI Insight*, *4*, e131712.

Castro, J., Maddern, J., Erickson, A., Caldwell, A., Grundy, L., Harrington, A. M., & Brierley, S. M. (2020). Pharmacological modulation of voltage-gated sodium (NaV) channels alters nociception arising from the female reproductive tract. *Pain*, *162*, 227–242.

Castro, J., Maddern, J., Grundy, L., Manavis, J., Harrington, A. M., Schober, G., & Brierley, S. M. (2021). A mouse model of endometriosis that displays vaginal, colon, cutaneous, and bladder sensory comorbidities. *The FASEB Journal*, *35*, e21430.

Ceccaroni, M., Clarizia, R., Roviglione, G., Bruni, F., Ruffo, G., Peters, I., De Placido, G., & Minelli, L. (2010). Deep rectal and parametrial infiltrating endometriosis with monolateral pudendal nerve involvement: Case report and laparoscopic nerve-sparing approach. *European Journal of Obstetrics, Gynecology, and Reproductive Biology*, *153*, 227–229.

Chen, H., Vannuccini, S., Capezzuoli, T., Ceccaroni, M., Mubiao, L., Shuting, H., Wu, Y., Huang, H., & Petraglia, F. (2021). Comorbidities and quality of life in women undergoing first surgery for endometriosis: Differences between Chinese and Italian population. *Reproductive Sciences*, *28*, 2359–2366.

Clark, A. K., Old, E. A., & Malcangio, M. (2013). Neuropathic pain and cytokines: Current perspectives. *Journal of Pain Research*, *6*, 803–814.

Dang, K., Lamb, K., Cohen, M., Bielefeldt, K., & Gebhart, G. F. (2008). Cyclophosphamide-induced bladder inflammation sensitizes and enhances P2X receptor function in rat bladder sensory neurons. *Journal of Neurophysiology*, *99*, 49–59.

Deberry, J. J., Schwartz, E. S., & Davis, B. M. (2014). TRPA1 mediates bladder hyperalgesia in a mouse model of cystitis. *Pain*, *155*, 1280–1287.

Decter, D., Arbib, N., Markovitz, H., Seidman, D. S., & Eisenberg, V. H. (2021). Sonographic signs of adenomyosis in women with endometriosis are associated with infertility. *Journal of Clinical Medicine*, *10*, 2355.

Deleo, J. A., & Yezierski, R. P. (2001). The role of neuroinflammation and neuroimmune activation in persistent pain. *Pain*, *90*, 1–6.

Dodds, K. N., Beckett, E. A., Evans, S. F., Grace, P. M., Watkins, L. R., & Hutchinson, M. R. (2016). Glial contributions to visceral pain: Implications for disease etiology and the female predominance of persistent pain. *Translational Psychiatry*, *6*, e888.

Dodds, K. N., Beckett, E. A. H., Evans, S. F., & Hutchinson, M. R. (2019). Spinal glial adaptations occur in a minimally invasive mouse model of endometriosis: Potential implications for lesion etiology and persistent pelvic pain. *Reproductive Sciences*, *26*, 357–369.

Echeverry, S., Shi, X. Q., & Zhang, J. (2008). Characterization of cell proliferation in rat spinal cord following peripheral nerve injury and the relationship with neuropathic pain. *Pain*, *135*, 37–47.

Eng, L. F., & Ghirnikar, R. S. (1994). GFAP and astrogliosis. *Brain Pathology*, *4*, 229–237.

Gautam, M., Prasoon, P., Kumar, R., Reeta, K. H., Kaler, S., & Ray, S. B. (2016). Role of neurokinin type 1 receptor in nociception at the periphery and the spinal level in the rat. *Spinal Cord*, *54*, 172–182.

Greaves, E., Horne, A. W., Jerina, H., Mikolajczak, M., Hilferty, L., Mitchell, R., Fleetwood-Walker, S. M., & Saunders, P. T. (2017). EP2 receptor antagonism reduces peripheral and central hyperalgesia in a preclinical mouse model of endometriosis. *Scientific Reports*, *7*, 44169.

Grundstrom, H., Gerdle, B., Alehagen, S., Bertero, C., Arendt-Nielsen, L., & Kjolhede, P. (2019). Reduced pain thresholds and signs of sensitization in women with persistent pelvic pain and suspected endometriosis. *Acta Obstetricia et Gynecologica Scandinavica*, *98*, 327–336.

Grundy, L., Erickson, A., & Brierley, S. M. (2019). Visceral Pain. *Annual Review of Physiology*, *81*, 261–284.

Grundy, L., Erickson, A., Caldwell, A., Garcia-Caraballo, S., Rychkov, G., Harrington, A., & Brierley, S. M. (2018). Tetrodotoxin-sensitive voltage-gated sodium channels regulate bladder afferent responses to distension. *Pain*, *159*, 2573–2584.

Grundy, L., Harrington, A. M., Castro, J., Garcia-Caraballo, S., Deiteren, A., Maddern, J., Rychkov, G. Y., Ge, P., Peters, S., Feil, R., Miller, P., Ghetti, A., Hannig, G., Kurtz, C. B., Silos-Santiago, I., & Brierley, S. M. (2018). Chronic linaclotide treatment reduces colitis-induced neuroplasticity and reverses persistent bladder dysfunction. *JCI Insight*, *3*, e121841.

Hanisch, U. K., & Kettenmann, H. (2007). Microglia: Active sensor and versatile effector cells in the normal and pathologic brain. *Nature Neuroscience*, *10*, 1387–1394.

Harrington, A. M., Brierley, S. M., Isaacs, N., Hughes, P. A., Castro, J., & Blackshaw, L. A. (2012). Sprouting of colonic afferent central terminals and increased spinal mitogen-activated protein kinase expression in a mouse model of chronic visceral hypersensitivity. *The Journal of Comparative Neurology*, *520*, 2241–2255.

Harrington, A. M., Caraballo, S. G., Maddern, J. E., Grundy, L., Castro, J., & Brierley, S. M. (2019). Colonic afferent input and dorsal horn neuron activation differs between the thoracolumbar and lumbosacral spinal cord. *American Journal of Physiology. Gastrointestinal and Liver Physiology*, *317*, G285–g303.

Honore, P., Rogers, S. D., Schwei, M. J., Salak-Johnson, J. L., Luger, N. M., Sabino, M. C., Clohisy, D. R., & Mantyh, P. W. (2000). Murine models of inflammatory, neuropathic and cancer pain each generates a unique set of neurochemical changes in the spinal cord and sensory neurons. *Neuroscience*, *98*, 585–598.

Hopperton, K. E., Mohammad, D., Trepanier, M. O., Giuliano, V., & Bazinet, R. P. (2018). Markers of microglia in post-mortem brain samples from patients with Alzheimer's disease: A systematic review. *Molecular Psychiatry*, *23*, 177–198.

Ikeda, H., Heinke, B., Ruscheweyh, R., & Sandkuhler, J. (2003). Synaptic plasticity in spinal lamina I projection neurons that mediate hyperalgesia. *Science*, *299*, 1237–1240.

Imai, Y., Ibata, I., Ito, D., Ohsawa, K., & Kohsaka, S. (1996). A novel gene iba1 in the major histocompatibility complex class III region encoding an EF hand protein expressed in a monocytic lineage. *Biochemical and Biophysical Research Communications*, *224*, 855–862.

Inserra, M. C., Israel, M. R., Caldwell, A., Castro, J., Deuis, J. R., Harrington, A. M., Keramidas, A., Garcia-Caraballo, S., Maddern, J., Erickson, A., Grundy, L., Rychkov, G. Y., Zimmermann, K., Lewis, R. J., Brierley, S. M., & Vetter, I. (2017). Multiple sodium channel isoforms mediate the pathological effects of Pacific ciguatoxin-1. *Scientific Reports*, *7*, 42810.

Ito, D., Imai, Y., Ohsawa, K., Nakajima, K., Fukuuchi, Y., & Kohsaka, S. (1998). Microglia-specific localisation of a novel calcium binding protein, Iba1. *Brain Research. Molecular Brain Research*, *57*, 1–9.

Jiang, Y., Castro, J., Blomster, L. V., Agwa, A. J., Maddern, J., Schober, G., Herzig, V., Chow, C. Y., Cardoso, F. C., De Souza, D., Franca, P., Gonzales, J., Schroeder, C. I., Esche, S., Reiner, T., Brierley, S. M., & King, G. F. (2021). Pharmacological inhibition of the voltage-gated Sodium Channel NaV1.7 alleviates chronic visceral pain in a rodent model of irritable bowel syndrome. *ACS Pharmacology & Translational Science*, *4*, 1362–1378.

Kettenmann, H., Hanisch, U. K., Noda, M., & Verkhratsky, A. (2011). Physiology of microglia. *Physiological Reviews*, *91*, 461–553.

Koninckx, P. R., Ussia, A., Adamyan, L., Wattiez, A., Gomel, V., & Martin, D. C. (2019). Pathogenesis of endometriosis: The genetic/epigenetic theory. *Fertility and Sterility*, *111*, 327–340.

Latremoliere, A., & Woolf, C. J. (2009). Central sensitization: A generator of pain hypersensitivity by central neural plasticity. *The Journal of Pain*, *10*, 895–926.

Laux-Biehlmann, A., D'hooghe, T., & Zollner, T. M. (2015). Menstruation pulls the trigger for inflammation and pain in endometriosis. *Trends in Pharmacological Sciences*, *36*, 270–276.

Lein, E. S., Hawrylycz, M. J., Ao, N., Ayres, M., Bensinger, A., Bernard, A., Boe, A. F., Boguski, M. S., Brockway, K. S., Byrnes, E. J., Chen, L., Chen, L., Chen, T. M., Chin, M. C., Chong, J., Crook, B. E., Czaplinska, A., Dang, C. N., Datta, S., et al. (2007). Genome-wide atlas of gene expression in the adult mouse brain. *Nature*, *445*, 168–176.

Leon-Rodriguez, A., Fernandez-Arjona, M. D. M., Grondona, J. M., Pedraza, C., & Lopez-Avalos, M. D. (2022). Anxiety-like behavior and microglial activation in the amygdala after acute neuroinflammation induced by microbial neuraminidase. *Scientific Reports*, *12*, 11581.

Li, T., Mamillapalli, R., Ding, S., Chang, H., Liu, Z. W., Gao, X. B., & Taylor, H. S. (2018). Endometriosis alters brain electrophysiology, gene expression and increases pain sensitization, anxiety, and depression in female mice. *Biology of Reproduction*, *99*, 349–359.

Liu, X. G., & Sandkuhler, J. (1998). Activation of spinal N-methyl-D-aspartate or neurokinin receptors induces long-term potentiation of spinal C-fibre-evoked potentials. *Neuroscience*, *86*, 1209–1216.

Liu, Z., Chen, S., Qiu, C., Sun, Y., Li, W., Jiang, J., & Zhang, J. M. (2018). Fractalkine/CX3CR1 contributes to endometriosis-induced neuropathic pain and mechanical hypersensitivity in rats. *Frontiers in Cellular Neuroscience*, *12*, 495.

Maddern, J., Grundy, L., Castro, J., & Brierley, S. M. (2020). Pain in endometriosis. *Front Cellular Neuroscience*, *14*, 590823.

Maddern, J., Grundy, L., Harrington, A., Schober, G., Castro, J., & Brierley, S. M. (2021). A syngeneic inoculation mouse model of endometriosis that develops multiple comorbid visceral and cutaneous pain like behaviours. *Pain*, *163*, 1622–1635.

Maillard, C., Cherif Alami, Z., Squifflet, J. L., Luyckx, M., Jadoul, P., Thomas, V., & Wyns, C. (2021). Diagnosis and treatment of Vulvo-perineal endometriosis: A systematic review. *Front Surgery*, *8*, 637180.

Malykhina, A. P., Qin, C., Greenwood-Van Meerveld, B., Foreman, R. D., Lupu, F., & Akbarali, H. I. (2006). Hyperexcitability of convergent colon and bladder dorsal root ganglion neurons after colonic inflammation: Mechanism for pelvic organ cross-talk. *Neurogastroenterology and Motility*, *18*, 936–948.

Mckinnon, B. D., Bertschi, D., Bersinger, N. A., & Mueller, M. D. (2015). Inflammation and nerve fiber interaction in endometriotic pain. *Trends in Endocrinology and Metabolism*, *26*, 1–10.

Monica Brauer, M., & Smith, P. G. (2015). Estrogen and female reproductive tract innervation: Cellular and molecular mechanisms of autonomic neuroplasticity. *Autonomic Neuroscience*, *187*, 1–17.

Morotti, M., Vincent, K., Brawn, J., Zondervan, K. T., & Becker, C. M. (2014). Peripheral changes in endometriosis-associated pain. *Human Reproduction Update*, *20*, 717–736.

Nimmerjahn, A., Kirchhoff, F., & Helmchen, F. (2005). Resting microglial cells are highly dynamic surveillants of brain parenchyma in vivo. *Science*, *308*, 1314–1318.

Old, E. A., & Malcangio, M. (2012). Chemokine mediated neuron-glia communication and aberrant signalling in neuropathic pain states. *Current Opinion in Pharmacology*, *12*, 67–73.

Osteen, J. D., Herzig, V., Gilchrist, J., Emrick, J. J., Zhang, C., Wang, X., Castro, J., Garcia-Caraballo, S., Grundy, L., Rychkov, G. Y., Weyer, A. D., Dekan, Z., Undheim, E. A., Alewood, P., Stucky, C. L., Brierley, S. M., Basbaum, A. I., Bosmans, F., King, G. F., & Julius, D. (2016). Selective spider toxins reveal a role for the Nav1.1 channel in mechanical pain. *Nature*, *534*, 494–499.

Palecek, J., Paleckova, V., & Willis, W. D. (2003). Postsynaptic dorsal column neurons express NK1 receptors following colon inflammation. *Neuroscience*, *116*, 565–572.

Palotai, M., Mike, A., Cavallari, M., Strammer, E., Orsi, G., Healy, B. C., Schregel, K., Illes, Z., & Guttmann, C. R. (2018). Changes to the septo-fornical area might play a role in the pathogenesis of anxiety in multiple sclerosis. *Multiple Sclerosis*, *24*, 1105–1114.

Peng, J., Gu, N., Zhou, L., Eyo, U. B., Murugan, M., Gan, W. B., & Wu, L. J. (2016). Microglia and monocytes synergistically promote the transition from acute to chronic pain after nerve injury. *Nature Communications*, *7*, 12029.

Polgár, E., Al Ghamdi, K. S., & Todd, A. J. (2010). Two populations of neurokinin 1 receptor-expressing projection neurons in lamina I of the rat spinal cord that differ in AMPA receptor subunit composition and density of excitatory synaptic input. *Neuroscience*, *167*, 1192–1204.

Raghavendra, V., Tanga, F. Y., & Deleo, J. A. (2004). Complete Freunds adjuvant-induced peripheral inflammation evokes glial activation and proinflammatory cytokine expression in the CNS. *The European Journal of Neuroscience*, *20*, 467–473.

Robbins, A., Sato, Y., Hotta, H., & Berkley, K. J. (1990). Responses of hypogastric nerve afferent fibers to uterine distension in estrous or metestrous rats. *Neuroscience Letters*, *110*, 82–85.

Saijo, K., & Glass, C. K. (2011). Microglial cell origin and phenotypes in health and disease. *Nature Reviews. Immunology*, *11*, 775–787.

Scholz, J., & Woolf, C. J. (2007). The neuropathic pain triad: Neurons, immune cells and glia. *Nature Neuroscience*, *10*, 1361–1368.

Sofroniew, M. V. (2014). Astrogliosis. *Cold Spring Harbor Perspectives in Biology*, *7*, a020420.

Soliman, A. M., Yang, H., Du, E. X., Kelley, C., & Winkel, C. (2016). The direct and indirect costs associated with endometriosis: A systematic literature review. *Human Reproduction*, *31*, 712–722.

Somigliana, E., Viganò, P., Rossi, G., Carinelli, S., Vignali, M., & Panina-Bordignon, P. (1999). Endometrial ability to implant in ectopic sites can be prevented by interleukin-12 in a murine model of endometriosis. *Human Reproduction*, *14*, 2944–2950.

Surrey, E. S., Soliman, A. M., Johnson, S. J., Davis, M., Castelli-Haley, J., & Snabes, M. C. (2018). Risk of developing comorbidities among women with endometriosis: A retrospective matched cohort study. *Journal of Women's Health (2002)*, *27*, 1114–1123.

Sutton, C. J., Ewen, S. P., Whitelaw, N., & Haines, P. (1994). Prospective, randomized, double-blind, controlled trial of laser

laparoscopy in the treatment of pelvic pain associated with minimal, mild, and moderate endometriosis. *Fertility and Sterility*, *62*, 696–700.

Taves, S., Berta, T., Chen, G., & Ji, R. R. (2013). Microglia and spinal cord synaptic plasticity in persistent pain. *Neural Plasticity*, *2013*, 753656.

Tsuda, M. (2016). Microglia in the spinal cord and neuropathic pain. *Journal of Diabetes Investigation*, *7*, 17–26.

Vega-Avelaira, D., Geranton, S. M., & Fitzgerald, M. (2009). Differential regulation of immune responses and macrophage/neuron interactions in the dorsal root ganglion in young and adult rats following nerve injury. *Molecular Pain*, *5*, 70.

Watkins, L. R., Milligan, E. D., & Maier, S. F. (2001). Glial activation: A driving force for pathological pain. *Trends in Neurosciences*, *24*, 450–455.

Zhou, Y. L., Zhou, S. Z., Li, H. L., Hu, M. L., Li, H., Guo, Q. H., Deng, X. M., Zhang, Y. Q., & Xu, H. (2018). Bidirectional modulation between infiltrating CD3(+) T-lymphocytes and astrocytes in the spinal cord drives the development of allodynia in monoarthritic rats. *Scientific Reports*, *8*, 51.

Zito, G., Luppi, S., Giolo, E., Martinelli, M., Venturin, I., Di Lorenzo, G., & Ricci, G. (2014). Medical treatments for endometriosis-associated pelvic pain. *BioMed Research International*, *2014*, 191967.

How to cite this article: Castro, J., Maddern, J., Erickson, A., Harrington, A. M., & Brierley, S. M. (2024). Peripheral and central neuroplasticity in a mouse model of endometriosis. *Journal of Neurochemistry*, *168*, 3777–3800. https://doi.org/10.1111/jnc.15843